Monitoring the plasmapause using geomagnetic field line resonances

F. W. Menk,[1] I. R. Mann,[2,3] A. J. Smith,[4] C. L. Waters,[1]
M. A. Clilverd,[4] and D. K. Milling[2,3]

Received 19 June 2003; revised 20 November 2003; accepted 9 February 2004; published 22 April 2004.

[1] This paper discusses the use of ground magnetometer data to derive plasma mass density profiles of the dayside plasmapause region with spatial and temporal resolution in the range 0.15–0.4 R_E and 20–60 min. This is achieved using cross-phase techniques to identify field line resonance signatures that are not apparent in power spectra. Under quiet conditions, mass density profiles do not show a distinct plasmapause and closely resemble electron density profiles for similar conditions. Under more active conditions the plasmapause can be clearly identified, and its width can be resolved in about 20% of the cases. Spatial integration effects smooth the mass density profiles near the plasmapause boundaries, while comparison of the mass and electron densities allows estimates of the heavy ion mass loading. Temporal variations in the plasmapause position and plasmaspheric density depletions are readily resolved. Sudden changes in solar wind conditions cause a redistribution of plasma within ~20 min, probably in response to penetration of the magnetospheric electric field into the plasmasphere. Field line resonances occur daily and provide a useful tool for investigating the plasmapause region, especially in conjunction with VLF whistler and in situ particle and imaging experiments. Furthermore, the extensive existing suites of magnetometer data permit retrospective studies of focus intervals. *INDEX TERMS:* 2740 Magnetospheric Physics: Magnetospheric configuration and dynamics; 2730 Magnetospheric Physics: Magnetosphere—inner; 2768 Magnetospheric Physics: Plasmasphere; 2752 Magnetospheric Physics: MHD waves and instabilities; 2794 Magnetospheric Physics: Instruments and techniques; *KEYWORDS:* field line resonance, plasmapause, ULF resonances

Citation: Menk, F. W., I. R. Mann, A. J. Smith, C. L. Waters, M. A. Clilverd, and D. K. Milling (2004), Monitoring the plasmapause using geomagnetic field line resonances, *J. Geophys. Res.*, *109*, A04216, doi:10.1029/2003JA010097.

1. Introduction

[2] This paper explores the use of ULF (~1–100 mHz) field line resonances (FLRs), measured with ground magnetometers, to examine the plasmapause region. This extends work in an earlier paper [*Menk et al.*, 1999] that used FLRs to monitor plasma density within the plasmasphere.

[3] The plasmapause has been extensively studied with VLF whistler techniques [e.g., *Carpenter and Park*, 1973; *Park et al.*, 1978] and satellite measurements [e.g., *Chappell et al.*, 1971; *Horwitz et al.*, 1990], and its average structure is now well established. The position of the plasmapause in the midnight sector depends directly on *Kp* [e.g., *Décréau et al.*, 1986] but on the dayside it is believed the plasmapause does not respond to changes in geomagnetic activity much faster than its corotation time from the previous nightside [*Carpenter*, 1970]. This is due to shielding of convection-driven electric fields by the region 2 current with a time constant of the order of an hour [*Senior and Blanc*, 1984]. However, recent satellite observations show that the response time of the dayside plasmapause may be almost as rapid as that on the nightside [*Bezrukikh et al.*, 2001; *Laakso and Jarva*, 2001].

[4] A variety of density features can occur near the plasmapause [e.g., *Moldwin et al.*, 1994; *Carpenter and Lemaire*, 1997; *Carpenter et al.*, 2000; *Sandel et al.*, 2001]. Storm-time radial density profiles show mesoscale structures that may include regions of cold detached plasma in the dayside and evening plasmatrough [*Chappell et al.*, 1971; *Maynard and Chen*, 1971]. *Horwitz et al.* [1990] presented a classification of six different types of plasma density profile, including cases where multiple plasmapauses and more complex structures are observed. About 60% of their density profiles exhibited features of this nature, mostly in the afternoon and evening sectors. The outer plasmasphere also exhibits considerable fine-scale (≤1000 km) structure, predominantly in the noon to dusk sector [e.g., *Chappell*, 1974; *Moldwin et al.*, 1995].

[5] Deep within the plasmasphere, plasma motion is generally controlled by flux transfer through ionosphere-

[1]School of Mathematical and Physical Sciences and Cooperative Research Centre for Satellite Systems, University of Newcastle, Callaghan, Australia.
[2]Physics Department, University of York, York, United Kingdom.
[3]Now at Physics Department, University of Alberta, Edmonton, Canada.
[4]British Antarctic Survey, Madingley Road, Cambridge, United Kingdom.

0148-0227/04/2003JA010097$09.00

protonosphere coupling and radial $\mathbf{E} \times \mathbf{B}$ drift of flux tubes driven by neutral winds in the ionosphere [*Poulter et al.*, 1984; *Saxton and Smith*, 1989]. Rapid fluctuations in solar wind or IMF conditions may transmit the magnetospheric dawn-to-dusk electric field into the inner magnetosphere [*Saxton and Smith*, 1991; *Balmforth et al.*, 1994], driving cross-L drifts until the shielding layer adjusts to the new conditions. A sudden northward turning of the IMF may therefore result in overshielding and the formation of a plasmaspheric shoulder or bulge [*Goldstein et al.*, 2002]. These effects cannot account for the observed erosion of the plasmasphere during and following storms [*Clilverd et al.*, 2000; *Chi et al.*, 2000].

[6] Empirical estimates of the plasmapause position are based on space-time averages that disguise the time variability of plasma in this region. There is a need for density measurements spanning a range of L shells and local times with good spatial and temporal resolution. Several techniques are available but each has limitations. Some of these are now outlined.

1.1. In Situ Measurements

[7] The local electron density can be determined from in situ plasma wave observations [*Mosier et al.*, 1973; *Gurnett et al.*, 1979]. However, the orbital motion of satellites makes it difficult to monitor the temporal evolution of localized features. For example, *Carpenter and Anderson* [1992] examined the magnetospheric density using (in part) upper hybrid wave data from the swept frequency receiver (SFR) on the ISEE 1 satellite with an orbital period of about 57 hours. By comparison, the CRRES satellite had a 10 hr orbital period, and its SFR experiment provided electron density data with spatial resolution of order 50 km at typical plasmapause distances. The experimental error in these densities is around 12% [*Carpenter et al.*, 2000].

[8] Direct measurements of ions and electrons have been reported by several workers [e.g., *Horwitz et al.*, 1984; *Moldwin et al.*, 1994]. However, positive charging of spacecraft surfaces in sunlight may exclude low energy ions from detectors [*Olsen*, 1982]. Much of the plasmaspheric ion population has energy $\leq$3 eV [*Moldwin et al.*, 1995]. This problem may be overcome by using negatively biased ion counters, yielding an uncertainty in ion density typically up to 30%. Furthermore, large ULF wave (e.g., Pc5) electric fields may cause particle motions into and out of spacecraft detectors, thus modulating particle count rates.

[9] The plasma mass density can also be estimated from in situ measurements of the field line eigenfrequency [e.g., *Takahashi and McPherron*, 1982]. However, the rapid motion of spacecraft results in spectral broadening and phase shear in on-board magnetometer data [*Anderson et al.*, 1989].

1.2. Satellite Imagers

[10] Optical remote sensing can provide important information on the structure of the plasmasphere [*Sandel et al.*, 2001]. In the case of the IMAGE spacecraft, the EUV images encompass the entire plasmasphere with spatial and temporal resolution of $\leq$0.1 R_E and 10 min. The images convey little spatial information along the line of sight, and information on the ion composition of the inner magnetosphere is necessary to accurately interpret the images during varying periods of geomagnetic activity levels. Ground-based ULF and VLF measurements can be used to intercalibrate the EUV Imager images [*Clilverd et al.*, 2003].

1.3. Ground-Based Measurements of VLF Whistlers

[11] Natural lightning-generated VLF whistler mode signals have been extensively used to study the electron density distribution in the inner magnetosphere. However, it is difficult to obtain continuous observations over a range of L shells using whistlers, since not all lightning events result in whistlers, and these whistlers propagate along field-aligned ducts that are most favorably located about 1.5 R_E inside the plasmapause [*Walker*, 1978]. The whistler ducts are formed by field-aligned electron density enhancements of order 5–10% [*Angerami*, 1970] and up to 40% [*Scarf and Chappell*, 1973], lending some uncertainty to electron density measurements.

[12] Due to ionospheric absorption, VLF whistler mode signals are difficult to detect when both ends of the flux tube are sunlit. VLF electron density measurements therefore favor night time, or high latitudes when one hemisphere is not sunlit. Furthermore, whistler mode signals only provide information on the electron density. Since the plasmaspheric refilling rate may be different for different ion species [*Singh and Horwitz*, 1992] it is also of interest to monitor heavy ion populations in the radiation belts.

[13] Whistler mode signals generated by continuously operating VLF transmitters can also be used to estimate the magnetospheric electron density [*Saxton and Smith*, 1989; *Clilverd et al.*, 1991]. This provides better local time coverage than with natural whistlers, but the frequencies available restrict this technique to $L \leq 2.7$.

[14] The purpose of this paper is to illustrate the use of ULF field line resonances to monitor spatial and temporal variations in the magnetosphere, in particular near the plasmapause. These resonances occur mostly on the dayside. Phase and amplitude comparison techniques were employed to measure the ULF field line eigenfrequency from the combined IMAGE and SAMNET magnetometer arrays during January and March 1998. The resultant radial plasma density profiles span most of the magnetosphere, and the mass densities are compared with VLF-derived electron densities. We show also that new information can be obtained on time variations in plasma density in response to sudden solar wind variations.

[15] ULF resonances can complement and extend whistler and spacecraft studies of the plasmapause region, because the basic data may be obtained from existing ground magnetometer arrays spanning a range of latitudes and longitudes, and because the resonances may be observed for many daylight hours on most days. Furthermore, since the field line eigenfrequency is determined by the plasma mass density rather than the electron density, ULF measurements may provide extra information on the heavy ion distribution. This is important because observations near geostationary orbit suggest that the O^+ density varies strongly during the solar cycle and with changing magnetic activity, while there is only a small effect on H^+ density [*Young et al.*, 1982]. Additionally, the O^+ concentration is

often enhanced by an order of magnitude or more near the plasmapause [*Roberts et al.*, 1987, and references therein].

2. Observations and Data Analysis

2.1. Detection of Field Line Resonances

[16] Techniques for the detection of FLRs were summarized by *Menk et al.* [1999, 2000]. It is assumed that an Alfvén eigenfrequency continuum exists throughout the magnetosphere, while discrete driven FLRs (characterized by a peak in power spectra) appear as a resonant enhancement in this continuum [*Mathie et al.*, 1999]. Over a suitably restricted range of latitudes properties of the local Alfvén resonance are determined by the leading order variations in amplitude and phase [*Southwood*, 1974]. The resonance may then be identified by the peak in H-component cross-power and cross-phase approximately mid-way between nearby latitudinally separated magnetometer stations. The diurnal pattern of resonance behavior is most clearly seen using dynamic cross-phase spectra [e.g., *Waters et al.*, 1991].

[17] The simultaneous signatures of a field line resonance between a poleward (P) and equatorward (E) station are:

[18] 1. a peak in the H-component cross-phase spectrum, $\Delta\phi_{EP}$;

[19] 2. a zero crossing in the H-component power difference spectrum, $H_P - H_E$;

[20] 3. a unity crossing in the H-component power ratio spectrum, H_P/H_E; and

[21] 4. a dip in the coherence spectrum.

[22] If the ground stations map to a region where the Alfvén velocity changes rapidly, the cross-phase response may include contributions arising from the local variations in Alfvén velocity as well as the local FLR. Near a steep plasmapause the Alfvén velocity passes through two turning points over a spatial scale of the same order as the resonance widths. Thus the assumption of a slowly varying background eigenfrequency profile is invalid, and two field lines mapping to either side of the plasmapause will show a reduced cross-phase [*Menk et al.*, 1999].

[23] *Vellante et al.* [2002] described a further polarization vector-based technique that has not been used here, and *Rees et al.* [2001] discussed wavelet-based filtering that may assist identification of the resonant frequency in cross-phase spectra, also not used here. Experience shows that the different methods listed above may indicate slightly different resonant frequencies. Following *Menk et al.* [1999, 2000], we therefore identified the resonant frequency as the frequency where the above criteria are most nearly simultaneously satisfied. The uncertainty is taken as the range of frequencies over which resonance signatures occur, plus the frequency resolution of the FFT (typically 0.3 mHz).

[24] It is also possible to identify the resonant frequency from single station data, where

[25] 1. the ratio or difference between the H- and D-component power exhibits a peak [e.g., *Vellante et al.*, 1993], and

[26] 2. there is a rapid change in phase between the H and D components.

[27] In the first case it is assumed that the resonance has greater amplitude in the H-component than the D-component (i.e., the wave modes are decoupled), while in the second case the rapid change in phase of the H component identifies the resonance.

2.2. Magnetometer Data and Mass Densities

[28] In order to monitor the radial plasma density distribution, we examined ULF FLRs during January and March 1998 using the combined IMAGE and SAMNET ground magnetometer arrays. Magnetic conditions during January were generally quiet (average $Kp \sim 1.5$), while March provided a sample of more disturbed conditions, including a $Kp = 7+$ magnetic storm.

[29] Data were obtained from 21 stations of the IMAGE (International Monitor for Auroral Geomagnetic Effects) array, spanning $3.3 < L < 15$ (56°N to 76°N) mostly between 15° and 27° geographic longitude. Further details on IMAGE are given by *Lühr et al.* [1998]. The data were sampled in geographic coordinates at 0.1 Hz (averaged from 1 s measurements) with a resolution of ~0.1 nT, and rotated into geomagnetic (H, D) coordinates before analysis.

[30] The SAMNET (Sub-Auroral Magnetometer NETwork) array [*Yeoman et al.*, 1990] was operated by the University of York and comprises digital fluxgate magnetometers that sample the geomagnetic H, D and Z components at 1.0 Hz with resolution <0.1 nT. We used data from 8 stations spanning $2.56 < L < 6.1$ near 358° and 20° geographic longitude. Some of the SAMNET and IMAGE stations are co-located, but the former have better time resolution. Local time at SAMNET and IMAGE is in the range LT = UT to LT = UT + 2 hr.

[31] Analysis of FLR activity involved inspection of high pass filtered ($f > 1$ mHz) time series and whole-day dynamic power, cross-power and cross-phase spectra to determine the presence of FLRs. This was done for all days using up to 20 combinations of station pairs. The dynamic spectra were usually computed with a 256-point (43 min, IMAGE) or 2048-point (34 min, SAMNET) FFT weighted by a Hanning window and stepping in increments of 30 or 300 points respectively. The actual spectra examined are in color and considerably clearer than the examples shown here.

[32] The resonant frequency was measured from discrete H-component FFT cross-power, coherence, power difference, power ratio, and cross-phase spectra on selected days. Examples of such discrete spectra are given by *Menk et al.* [1999, 2000] and *Rees et al.* [2001]. The spectra were computed over time windows mostly between 30 and 60 min long, the shorter windows being used under more active conditions. This was done for many days in January and March, but this paper only presents illustrative examples from 1, 8 and 11 January. Discrete spectra were examined from typically 15 station pairs for selected time intervals. In addition, discrete spectra of the H- and D-component cross-power, coherence, power difference and cross-phase were also examined for 11–12 single stations at the same times on these days, in order to provide measurement points where there were no suitably spaced station pairs.

[33] Such discrete spectra are only a 'snapshot' approximation to the actual spectrum, and a different FFT window function may change details within a spectrum

but not the underlying important features. This is because of the variability in pulsation signals on time scales comparable to the FFT length, probably related to the wave packet nature of the pulsations. This variability tends to be averaged out in the whole-day spectra. Therefore start and end times of discrete spectra were chosen as far as possible to avoid the mixing of wave packets, and the whole-day dynamic spectra were used to aid the interpretation of temporal variations in resonant frequency. *Vellante et al.* [2002] found that for low latitude FLRs the cross-phase and cross-power information is not affected by the choice of start and end times.

[34] Mass densities were calculated from the measured resonant frequencies using expressions given by *Taylor and Walker* [1984] and *Walker et al.* [1992]. These assume decoupled toroidal mode oscillations and yield essentially identical results to the models described by *Orr and Matthew* [1971]. We represent the mass density in the equatorial plane (where the magnetic field strength and hence Alfvén velocity along a field line generally reach a minimum) by a model distribution of the form R^{-p}. This is invalid for very low or high latitude field lines, because of mass loading by ionospheric heavy ions, and field line distortion. At higher latitudes the geomagnetic field was therefore represented by the Olson-Pfitzer approximation described by *Singer et al.* [1981] or by the *Tsyganenko and Stern* [1996] model, T96. It is also assumed that the plasma is collisionless.

[35] The choice of power law describing the radial density variation has been discussed by many authors [e.g., *Gul'yel'mi*, 1966; *Denton and Gallagher*, 2000; *Goldstein et al.*, 2001]. Following previous work, we used $p = 3$ (corresponding to diffusive equilibrium at low latitudes) inside the plasmasphere, and $p = 4$ (corresponding to a collisionless distribution) outside the plasmapause. The calculated mass density is relatively insensitive to the actual choice of power law [*Orr and Matthew*, 1971; *Walker et al.*, 1992]. In their global core plasma model, *Gallagher et al.* [2000] represented the plasmaspheric density by a power law expression whose leading order term is $-0.79L + 5.3$. Although we have used a simpler functional form, this does not affect the determination of the plasmapause position.

[36] The uncertainty in our calculated mass densities depends on uncertainty in the frequency measurement through dependence of time of flight on the Alfvén velocity, and is typically of order 15%. This is represented by error bars in plots shown later. Uncertainties due to the R^{-p} model approximation are ignored. Since the guided poloidal mode eigenfrequency is ~30% lower than our assumed purely toroidal mode oscillations, wave mode coupling may cause the mass density to be slightly underestimated. This uncertainty is also not represented in the plots. The equatorial mass density can also be determined from comparison of toroidal mode resonance harmonics [*Schulz*, 1996]. That method requires observed frequencies to be accurate to ~6% in order to obtain equatorial mass density with a precision of 30% [*Denton and Gallagher*, 2000], and has not been used here.

[37] We also used magnetometer data from the 210° array for a particular case study. For this purpose we obtained 1-min averages of H-component digital data originally sampled at 1 Hz from 11 stations lying near the 210° magnetic meridian, and spanning $1.00 < L < 8.5$ (4°N to 70°N) latitude. Details on the array appear in *Yumoto et al.* [1992].

2.3. VLF Data

[38] Equatorial electron densities (N_{eq}) were estimated for L shells beyond $L \sim 2.0$ using natural VLF whistlers recorded at Halley, Antarctica (geographic 76°S, 27°W, $L = 4.3$). Halley VLF data are recorded for one minute in each 15. The whistlers are typically observed up to but not beyond the plasmapause, propagating in ducts of enhanced density with cross-L width of order 300–400 km in the equatorial plane [*Angerami*, 1970]. The technique of *Ho and Bernard* [1973] was used to determine the nose frequency and the travel time to the nose, and electron densities were then obtained using a diffusive equilibrium model for the plasma distribution. The error in evaluating N_{eq} is of order 5% [*Ho and Bernard*, 1973; *Park*, 1973]. Whistler studies from Halley were recently reviewed by *Smith* [2001].

3. Results

3.1. 1 January 1998

[39] We first present illustrative results from 1 January 1998. This is a magnetically quiet day ($Kp \leq 1.3$, $\Sigma Kp = 7.7$) following almost three weeks of very quiet conditions, except for 30 December 1997, when Kp twice reached 4.7. On 31 December ΣKp was 5.7.

[40] Whole-day dynamic cross-phase spectra for four representative station pairs are shown in Figure 1. The FLR appears as a narrow horizontal band from around 02–17 UT (about 03–18 LT), ranging from 3–4 mHz for MUO:KIL (top panel) to ~8 mHz for NUR:HAN (bottom). Additional broadband structure is present at higher frequencies, from ~14–45 mHz for MUO:HAN to ~25–35 mHz for NUR:HAN. This activity is not related to the FLRs that occur at lower frequencies and is not discussed further in this paper. The spectra shown in Figure 1 are similar to those presented by *Milling et al.* [2001] for similar latitudes, and the local times over which the resonances are observed are fairly typical.

[41] Time series records from several stations for the interval 0700–0800 UT are presented in Figure 2a. The time series were high pass filtered at 1 mHz and show that pulsation activity seems to fall into four latitude-dependent categories. At the lower latitudes (≤60° CGM, $L \leq 4$), pulsations are weak and of irregular appearance. Signals are somewhat larger around 63–67° latitude ($4 < L < 7$), and the largest amplitudes occur ~71–74° latitude. Pulsation activity at the highest latitude stations (≥75°) is less intense and has somewhat different structure to that at lower latitudes.

[42] Figure 2b shows power spectra from several of these stations for the same interval presented above. For convenience the spectra have been spaced by 20 dB (one tick mark). There are no obvious systematic latitude-dependent changes in the position of spectral peaks. Rather, peaks in power are present at several common frequencies, in particular ~3–4 mHz and 30 mHz, across a range of latitudes. This highlights the importance of using cross-phase type techniques to detect FLRs, rather than simply choosing the frequency where power peaks. The D-component spectra (not shown) generally have lower power and also display no obvious frequency-latitude relationship.

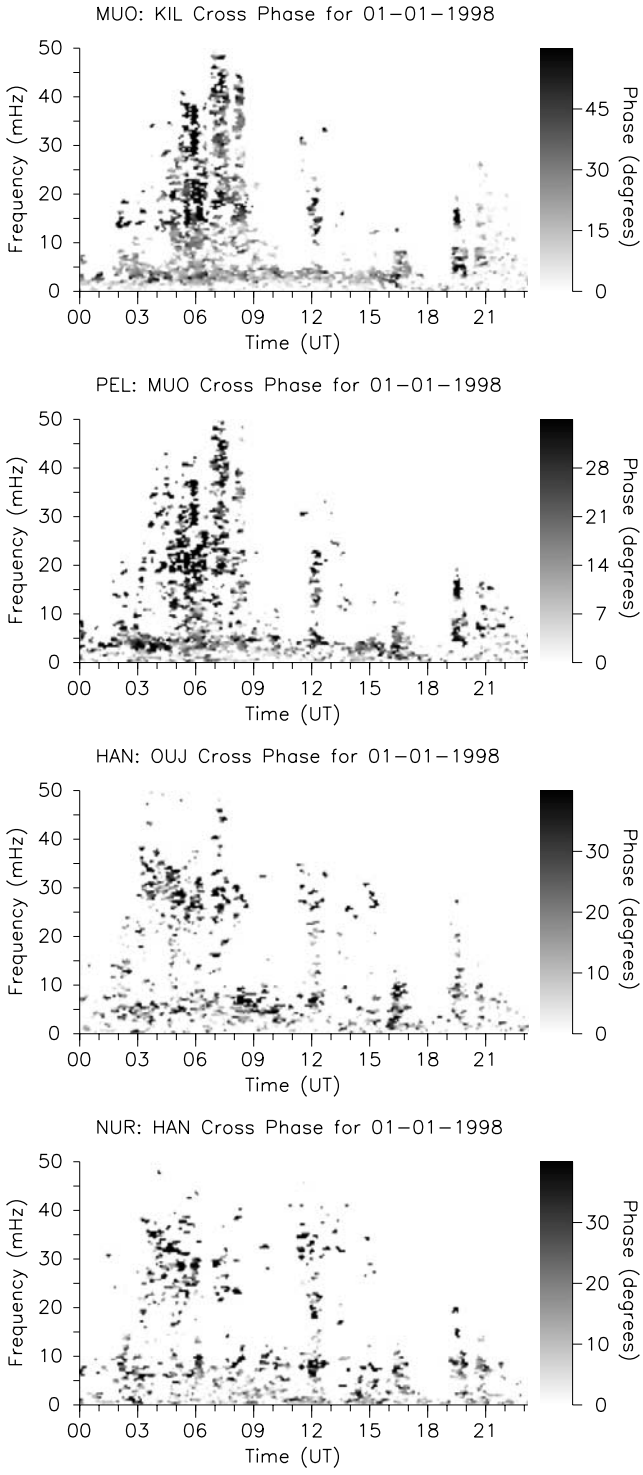

Figure 1. Whole-day dynamic cross-phase spectra for 1 January 1998. Station midpoints are, from top to bottom, near L = 5.8 (MUO:KIL; station separation ~110 km), L = 5.3 (PEL:MUO; 130 km), L = 4.0 (HAN:OUJ; 180 km), and L = 3.7 (NUR:HAN; 145 km). The field line resonance is present as a narrow band below 10 mHz.

[43] Measurements of the resonant frequency (from discrete spectra as described in section 2.2) between 0700 and 0800 UT are summarized in the top panel of Figure 3. Filled circles denote the mean of cross-phase, power difference and H/H power ratio values between station pairs, and open circles represent the result of single station H/D power ratio measurements. Error bars are comparable to the symbol size at lower latitudes. The vertical arrows indicate the approximate expected plasmapause position, after *Orr and Webb* [1975]. It is clear that the resonant frequencies measured by the two-station cross-phase/power comparison and single station power ratio methods fit a smoothly varying profile. The expected plasmapause position near L = 5.4 corresponds to a small increase in resonant frequency. Slightly larger error bars in this region result from frequency spread in the cross-phase, power difference and power ratio signatures.

[44] The bottom panel in Figure 3 depicts plasma mass densities derived from these resonant frequencies, where the symbols have the same meaning as before. The mass density profile resembles an electron density profile shown by *Carpenter and Anderson* [1992] for a day with similar *Kp* history (day 217). For comparison, the dotted line in Figure 3 represents the *Carpenter and Anderson* [1992] empirical electron density model for a saturated plasmasphere including annual, seasonal and solar cycle effects. Our mass density profile shows somewhat higher values at low L and lower values near and beyond the expected plasmapause position, as expected under the prevailing conditions.

[45] Also shown in the bottom panel of Figure 3 are two electron density values obtained from Halley whistler observations near 0905 UT but 2–4 hours west of the magnetometer stations. Each symbol and the associated error bars represents the average and range of 5 separate whistler measurements.

[46] Mass density determinations for this day are summarized in Figure 4. These are based on resonant frequencies measured each hour from IMAGE/SAMNET and stations spanning 51–69° geomagnetic latitude. For convenience the profiles have been separated vertically by one order of magnitude. No distinct plasmapause is present at any time, although density perturbations are evident around L = 4, especially after noon. The two filled circles mapping to the 07 LT profile represent the VLF electron density measurements. There was no significant change in solar wind pressure over the times shown.

3.2. 11 January 1998

[47] This day followed a short *Kp* = 6+ disturbance on 7 January and is typical of post-disturbed conditions. The D_{st} index dropped from +6 nT at 15–16 UT on 6 January to a minimum of −77 nT at 04–05 UT on 7 January, and by 11 January had recovered to pre-disturbance values. Whole-day dynamic power and cross-phase spectra (not presented) show sustained pulsation activity and FLRs at the IMAGE and SAMNET stations for much of this day. Power levels were higher than on 1 January.

[48] The variation in resonant frequency with latitude at four time intervals on 11 January is illustrated in Figure 5a. These intervals are representative of daytime activity on this day. The measurements were obtained from static spectra over time windows typically 40 min long at lower latitudes and 60 min at higher latitudes. Error bars with no corresponding data points denote instances where no single resonance signature was evident, but possible resonance

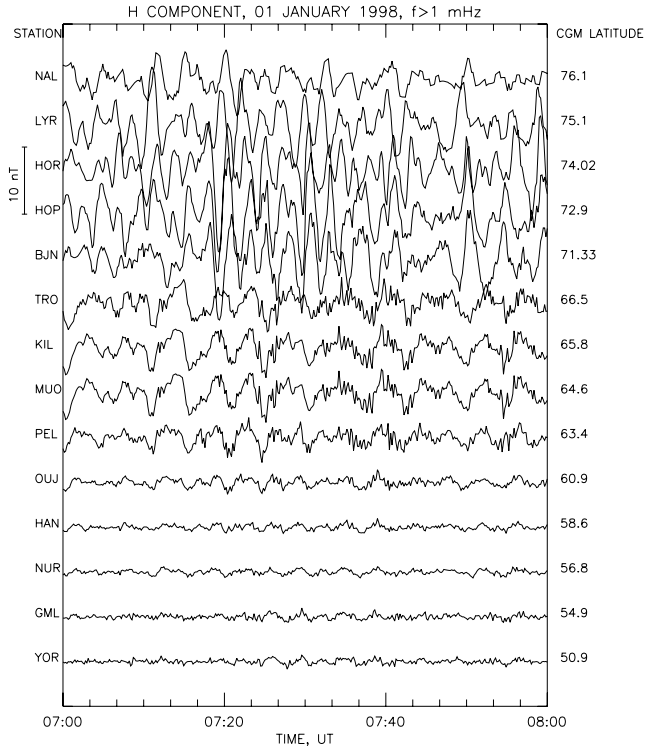

Figure 2a. Stacked H-component time-series records from representative SAMNET and IMAGE stations for 0700–0800 UT, 1 January 1998. LT is in the range UT to UT + 2.

signatures spanned a range of frequencies. These measurements are mostly at higher frequencies and appear to be harmonics of the fundamental FLR. Data points appearing along the latitude axis at 1 mHz frequency indicate cases where no resonance signature was apparent in the individual spectra. Notional lines of best fit have been drawn for illustrative purposes.

[49] The 0600–0700 UT resonant frequency profile (top panel) decreases smoothly from 21 mHz at $L = 2.5$ to about 6 mHz near $L = 5.1$, before increasing to about 10 mHz at $L = 5.4$ then decreasing beyond that. Measurements from the two-station and single-station FLR detection techniques are again self-consistent. Turning points in the profile are indicated by the absence of resonance signatures at $L = 4.8$ and $L = 5.7$.

[50] The second panel shows a similar frequency-latitude structure for 0900–1000 UT, except that: (a) resonance frequencies are generally lower at lower latitudes; (b) there is some irregularity in the frequencies around $L = 3.6$; (c) the frequency peak has moved equatorward to $L = 5.1$; and (d) the maximum frequency of this peak has increased to around 15 mHz. The peak has moved further equatorward by 1200–1300 UT. Finally, by 1500–1600 UT the irregularity around $L = 3.7$ has become more pronounced, and the peak has broadened and flattened.

[51] Plasma mass density profiles corresponding to these frequency plots are presented in Figure 5b. At 0600–0700 UT (top panel) there is an order of magnitude decrease in mass density between $L = 4.4$ and $L = 5.4$. This is around the plasmapause latitude predicted by the *Orr and Webb* [1975] estimate (and indicated by the vertical arrow). It is not possible to precisely measure the plasmapause latitude, but it is most likely near $L = 5.2$, between where the cross-phase signatures are suppressed. Elsewhere, in the plasmasphere and plasmatrough, the mass densities fit a smooth profile within experimental uncertainty.

[52] The plasma mass density profile for 0900–1000 UT is generally similar, except that: (a) densities are a bit higher at lower latitudes; (b) there is an anomalous decrease in density (by a factor of about 2.5) near $L = 3.6$; (c) the plasmapause is now most likely around $L = 4.8$, at the predicted location; and (d) the density just poleward of the plasmapause is lower than before. By 1200–1300 UT the plasmapause gradient appears to be shallower, due to slightly higher poleward densities, and it is significantly equatorward of its predicted location ($L = 4.4$ compared to $L = 5.2$), suggesting the usual outward diurnal movement is not evident. The density decrease near $L = 3.6$ is again present.

[53] Finally, by 1500–1600 UT the plasmapause appears to have moved further equatorward and become even shallower. However, a plateau has developed in the density-latitude profile, extending inward from the expected plasmapause latitude, between about $L = 4.8$ and $L = 6.8$. The plasmapause is probably around $L = 4.3$. Mass densities in

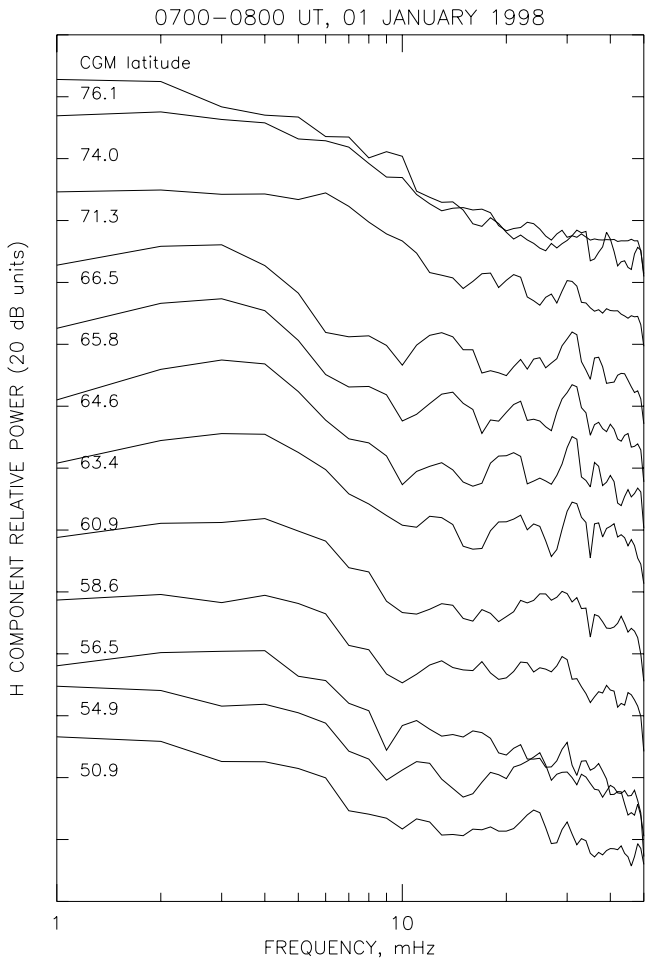

Figure 2b. Stacked H-component power spectra from representative SAMNET and IMAGE stations for 0700–0800 UT, 1 January 1998.

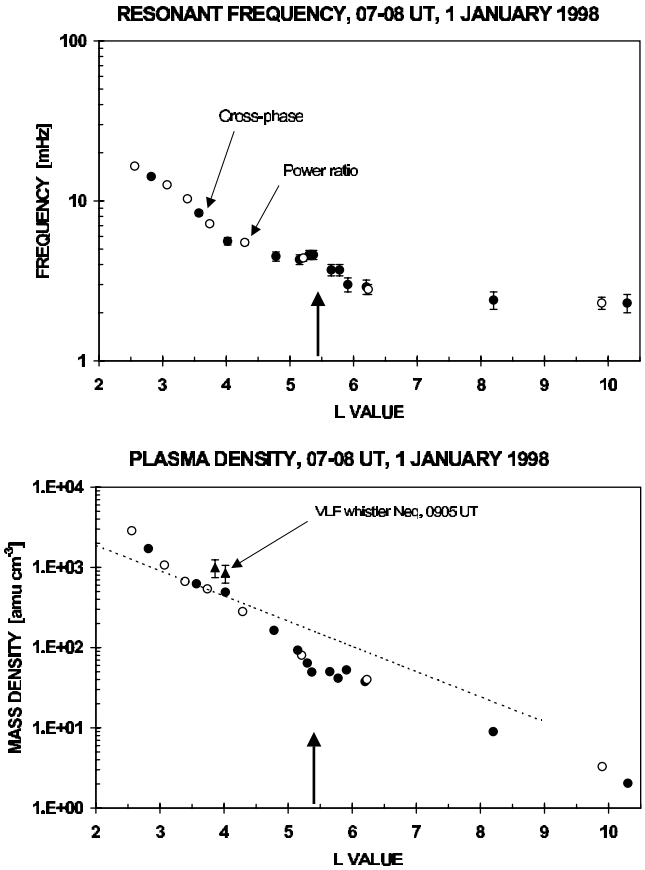

Figure 3. Field line resonance frequencies (top panel) and plasma mass densities (bottom) for 0700–0800 UT, 1 January 1998. Filled and closed circles denote two-station and single station measurements respectively. Arrows indicate predicted plasmapause latitude. In the bottom panel, triangles represent whistler-derived electron densities at 0905 UT, and dotted line shows *Carpenter and Anderson* [1992] model profile for a saturated plasmasphere.

the plasmasphere are significantly higher than earlier in the day. No resonance signature is now identifiable by the pair of stations centered on $L = 3.6$. This means that the irregularity evident earlier has evolved to form a more localized structure whose radial width, projected to the ground, is comparable to the station separation.

[54] No whistlers were present in the Halley VLF data on this day and therefore no comparisons with electron density data are possible. During the times of interest the solar wind velocity and pressure measured by the WIND spacecraft were within the range 330–380 km s^{-1} and 1.5–3.5 nPa, and B_z fluctuated between maximum ranges of +4 and −8 nT. The most significant southward turnings occurred at the magnetopause near 0533, 1005, 1143, 1504 and 1555 UT.

3.3. 8 January 1998

[55] This day follows the geomagnetic disturbance discussed above but ΣKp was only 14.7. Pulsation power levels were about 20 dB higher than on quiet days, and power spectra (not shown here) exhibit clear peaks. Some of these are latitude-dependent, but there are also peaks at common frequencies spanning many stations. The spectra do not display any obvious frequency-latitude trend identifying the plasmapause location.

[56] Well-defined resonance signatures are present most of this day in cross-phase spectra (also not presented here) across the entire IMAGE/SAMNET array. The spectra show unusually enhanced resonant frequencies between about 0800 and 1200 UT. A positive excursion of 7 nT occurred in D_{st} at 10–11 UT, indicating a sudden compression of the magnetosphere. Using an equation presented by *Farrugia et al.* [1989] indicates the magnetopause moved from $L = 13.1$ at 0800 UT to $L = 9.7$ at 1000 UT. H-component magnetograms from stations of the 210° array show that two global impulses occurred at 0831 UT and 1017 UT.

[57] The temporal variation in plasma mass density for selected SAMNET/IMAGE station pairs is illustrated in the

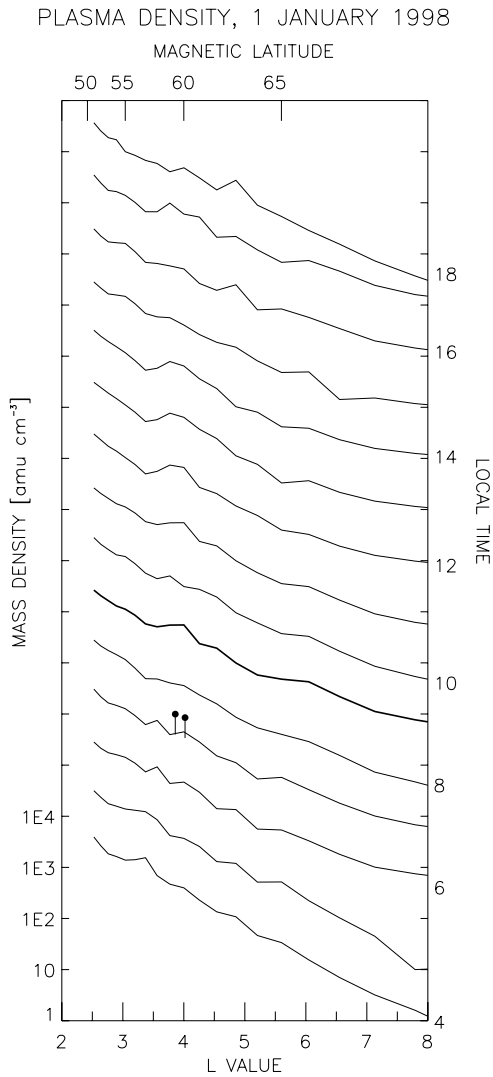

Figure 4. Variation of ULF-derived plasma mass density with latitude and time on 1 January 1998. Filled circles represent VLF electron density measurements at 0905 UT, and heavy line represents profile closest in time to that shown in Figure 3.

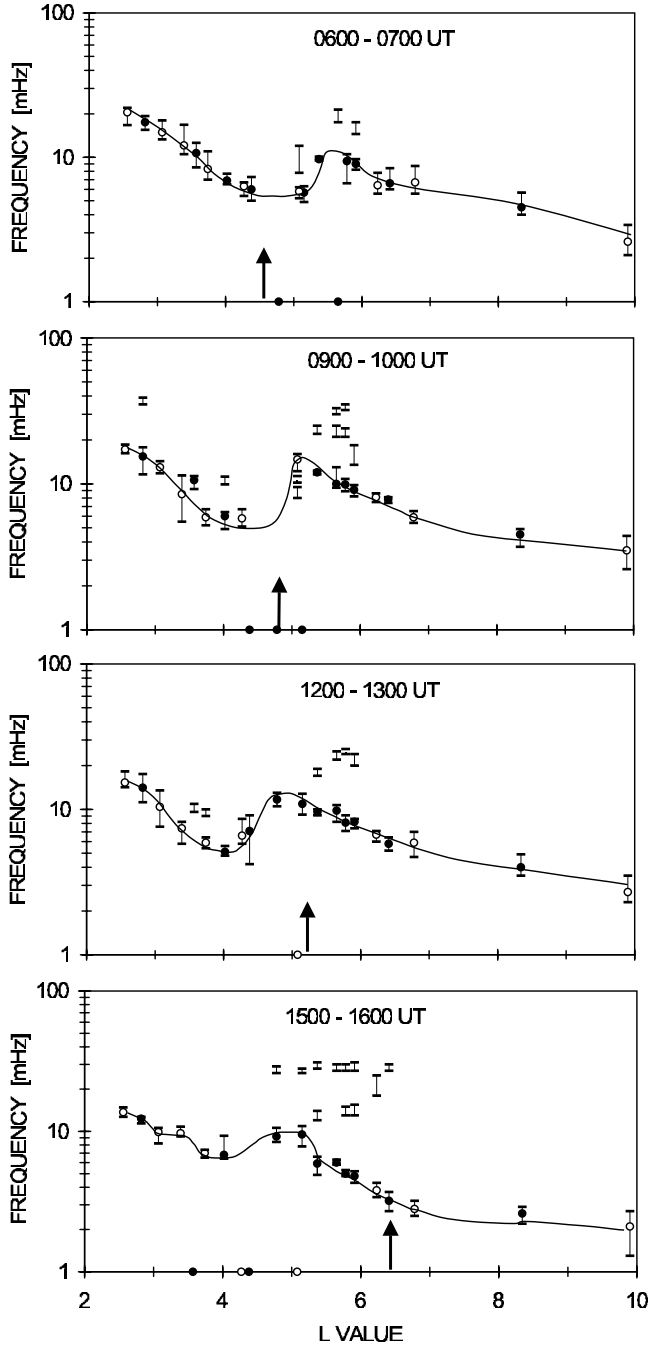

Figure 5a. Variation of resonant frequency with latitude on 11 January 1998, between 0600–0700 UT (top panel), 0900–1000 UT, 1200–1300 UT, and 1500–1600 UT (bottom). Symbols have the same meaning as in Figure 3.

top panel of Figure 6. Densities were calculated using the Olson-Pfitzer magnetic field model for measurements of the resonant frequency from discrete 30-min spectra that were stepped in 20-min increments. Mass densities calculated with the T96 model (shown later) are somewhat higher but display similar trends. The second panel shows the IMF B_z component, measured by the WIND spacecraft and with an appropriate propagation lag to the ground included. The third panel similarly presents the solar wind velocity, and the bottom panel the solar wind pressure. Two solar wind pressure enhancements are apparent, near 0830 UT and 1020 UT, and are identified by vertical dotted lines. The first coincides with a strong decrease in B_z, although this does not become clearly southward.

[58] The profiles in the top panel of Figure 6 show that between ~0830 and 1030 UT mass density appeared to decrease by a factor of about 3 for $L > 4$, with a smaller decrease for $L = 3.6$ and none for $L < 3$. Diamonds and filled circles denote Halley VLF electron densities for $L = 2.6$ and $L = 3.6$ ducts respectively, at the same UT but 25–50° west

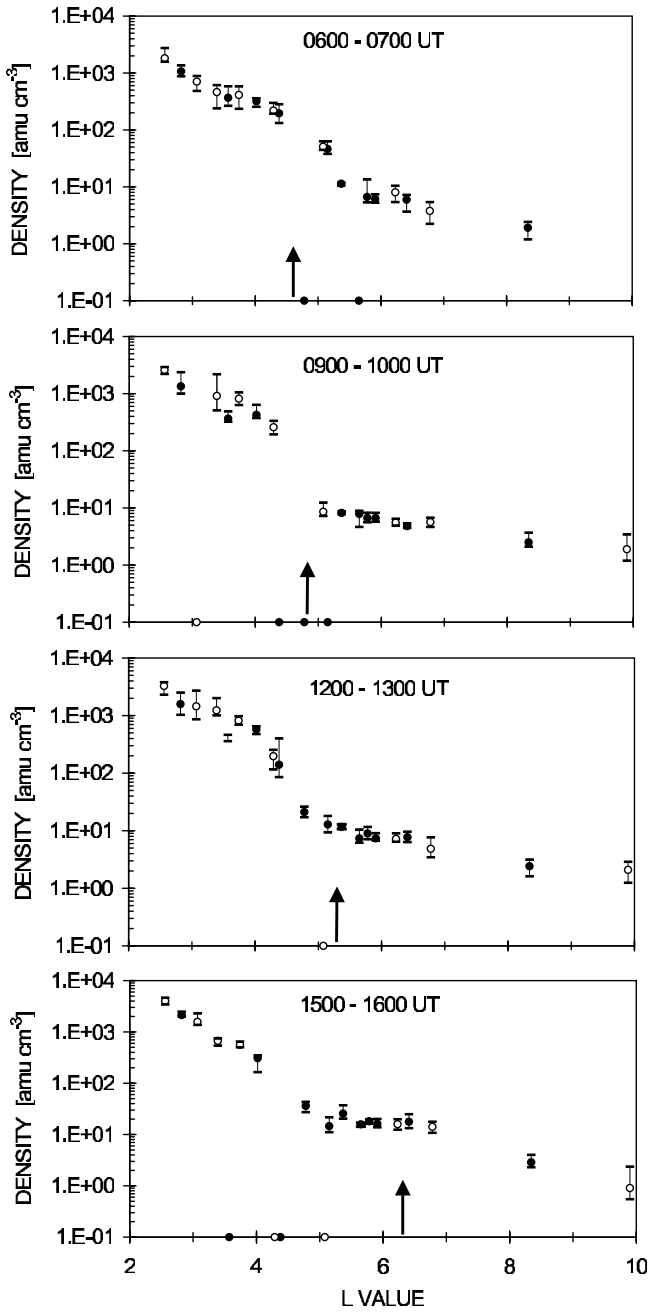

Figure 5b. Mass density profiles for times shown in Figure 5a.

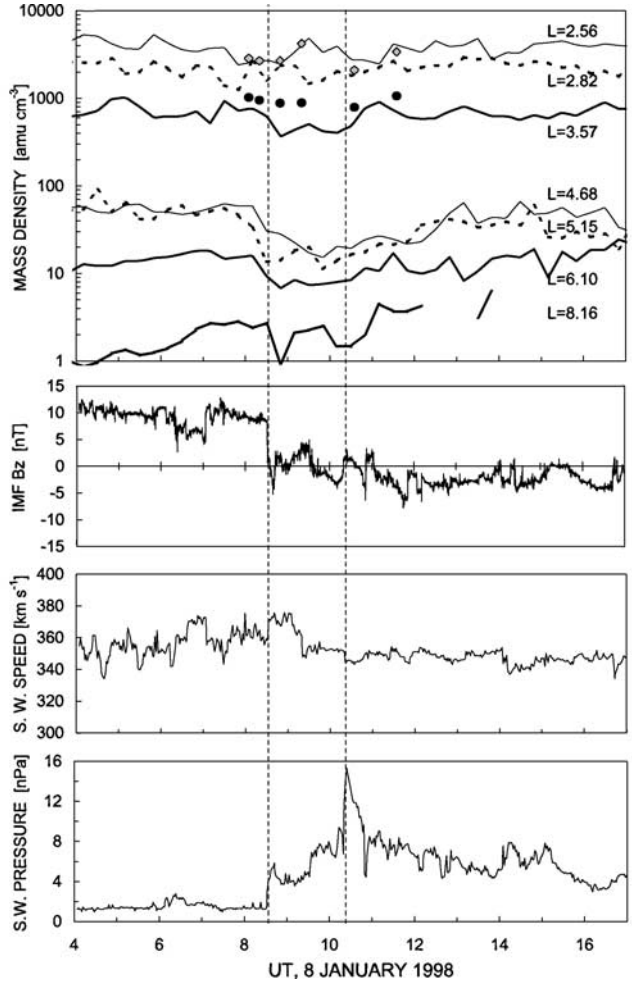

Figure 6. Top panel: Plasma mass density at selected latitudes on 8 January 1998 (LT = UT to UT + 2). Also shown are VLF electron densities (LT $\sim$ UT $-$ 2) from L = 3.0 (diamonds) and L = 3.6 (filled circles). Second panel: Interplanetary magnetic field B_z component measured by the WIND spacecraft, with a suitable propagation lag included. Third panel: Solar wind speed from WIND spacecraft. Bottom panel: Solar wind pressure measured by WIND. Vertical dotted lines indicate times of sudden pressure enhancements.

of the magnetometers. The L = 2.6 electron and mass densities show similar variation with UT, although this is not as clear for the L = 3.6 measurements.

[59] Next we consider frequency-latitude profiles, measured using 40-min long spectra centered on each hour from 0720 UT to 1220 UT (Figure 7a). For clarity no distinction is made between cross-phase, power comparison, or single station power ratio values. The profiles show complicated, dynamic behavior between L = 3 and L = 7. The position and size of the frequency peak, and the frequency profile equatorward of this peak, change significantly from one hour to the next. Temporal variations occurring within a spectral window result in large uncertainties. The actual plasmapause position, indicated by the latitude where the resonant frequency suddenly changes, moves from L = 5.1 to L = 4.0 during the times spanned by the profiles, and is always well equatorward of the expected plasmapause latitude represented by the vertical arrows.

[60] The corresponding plasma density profiles calculated using the T96 magnetic field model (i.e., including the effect of solar wind and D_{st} variations) are shown in Figure 7b in the same format as Figure 4. At 1020 UT solar wind pressure exceeded the range of T96 input parameters and therefore for this profile the solar wind pressure has been set to 10 nPa instead of the actual peak pressure of 15.3 nPa. Since the profiles have been drawn by simply connecting measurement points they probably underestimate the actual plasmapause gradient. Nevertheless, it is clear that the plasmapause is well equatorward of its expected location (L = 6–7) and appears to move generally equatorward, with significant changes in shape between 0820 and 0920 UT, i.e., after the initial solar wind impulse. Density fluctuations are also apparent around L = 5–6.5.

[61] Figure 7b also includes Halley VLF electron density observations, denoted by filled circles. Each point represents the average of several measurements near the indicated UT. The electron densities generally exhibit a similar variation in latitude with UT as the mass densities.

[62] Further information on the UT control of plasmaspheric density on this day is provided in Figure 7c, which compares the proportional change in observed electron density (filled circles), observed resonant frequency (dotted line), and calculated mass density, between 0820 UT and 0920 UT on 8 January. These times straddle the increase in solar wind pressure from 1.3 to $\sim$4.6 nPa. The IMF B_y and D_{st} remained essentially constant, and the plasmapause remained near L = 4.3 (Figure 7b) during these times. The plot shows that the change in mass density is almost a mirror image of the change in resonant frequency, despite the changes in field line configuration that accompany the varying solar wind conditions. After the 0831 UT solar wind enhancement, mass and electron densities generally increased inward of L < 3.3 and decreased for L > 3.3. The largest depletions in mass density occurred near the plasmapause ($L \sim$ 4.3) and in the plasmatrough. Between L = 3.3–4.0 mass density decreased more than twice as much as electron density, and between L = 3.0 and L = 3.3 the increase in mass density was much greater than that in electron density. However, there was a strong increase in electron density for L < 3.0.

[63] The observations for 8 January are not an isolated example. Temporal variations in resonant frequency are easily identified in whole-day dynamic cross-phase spectra, and similar behavior has been observed on other days in association with sudden changes in solar wind pressure. One such day is 31 January 1998, when ULF-derived mass densities increased (decreased) inward of (beyond) L = 3.5 immediately after sudden increases in solar wind pressure in the local evening sector.

3.4. 8–19 March 1998

[64] We now examine the plasmapause shape and location during a magnetic storm cycle. The top panel of Figure 8 shows mass density profiles at 12 UT for each day of 8–19 March. Tick marks on the x-axis correspond

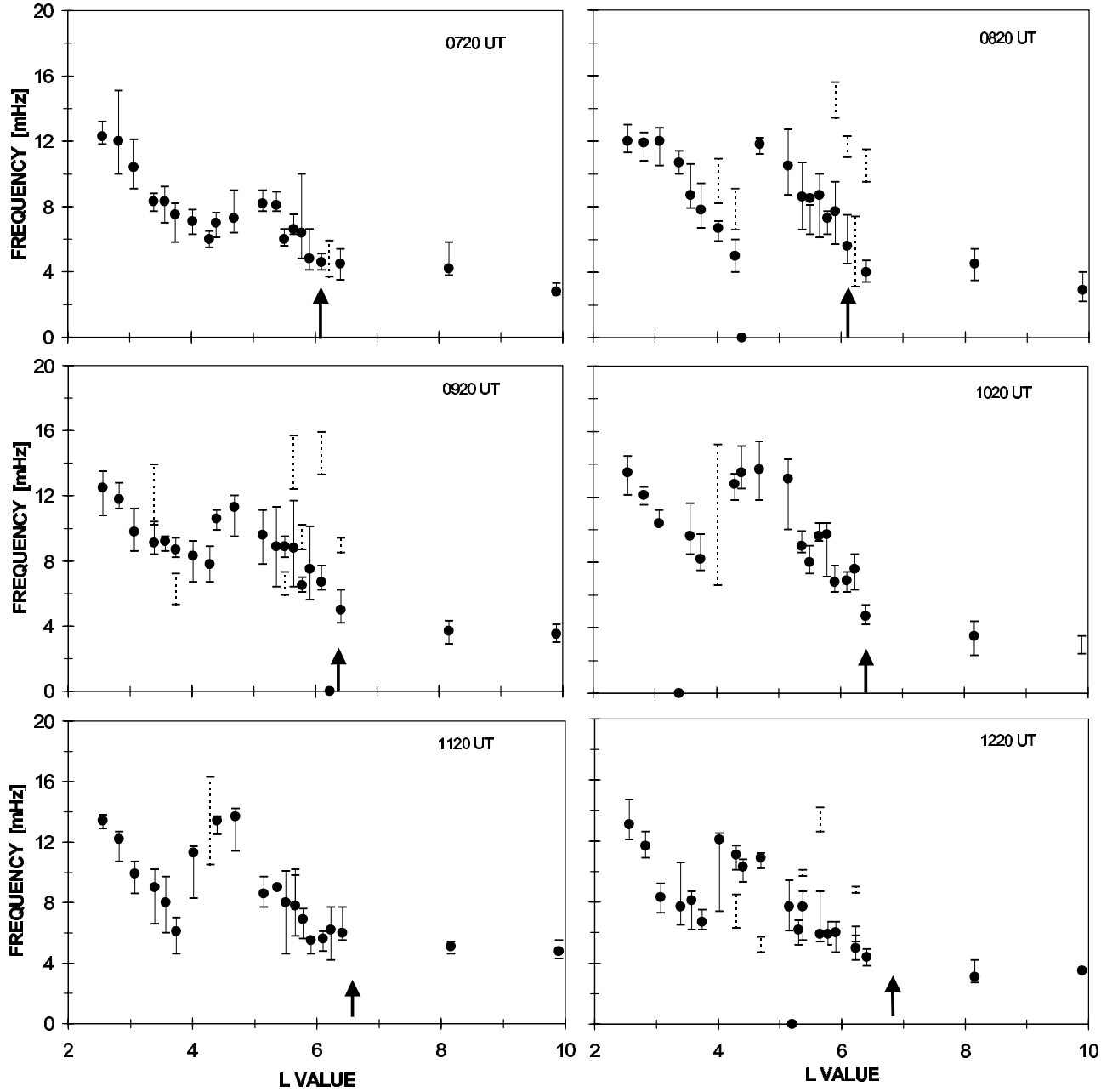

Figure 7a. Variation of resonant frequency with latitude on 8 January 1998, between 0720 UT (top left) and 1220 UT (bottom right). Symbols have the same meaning as in Figure 3.

to a step of $L = 1$, and each date label is at $L = 6$. Solid lines represent profiles for odd-numbered days. The bottom panel shows *Kp* over these days.

[65] This figure clearly illustrates the evolution of the dayside plasmapause with magnetic activity. For example, on 7 March no plasmapause is evident, while small, irregular density variations are present around $L = 4-5$ on 8, 9 and 10 March. The increase in *Kp* over 10–11 March results in significantly lower mass densities for $L > 3$ at 1200 UT on 12 March, consistent with the plasmapause having moved to $L \leq 3.0$. A well-defined plasmapause is present around $L = 3.4$, 4.2, and 4.2 on 12, 13 and 14 March. A large, steep plasmapause is present around $L = 3.8-4.0$ on 15 March; over the next few days this decays to form two density gradients, until by 19 March no clear plasmapause remains.

4. Discussion

4.1. Identification of the Plasmapause Using FLRs

[66] The cross-phase and power comparison techniques are powerful tools for the detection of FLRs, and permit the estimation of radial plasma density profiles using ground magnetometer data and suitable density and magnetic field models. However, there are a number of complicating issues. These are discussed below with reference to the model plasma density and eigenfrequency profiles shown in Figure 9. The profiles are based on observations for

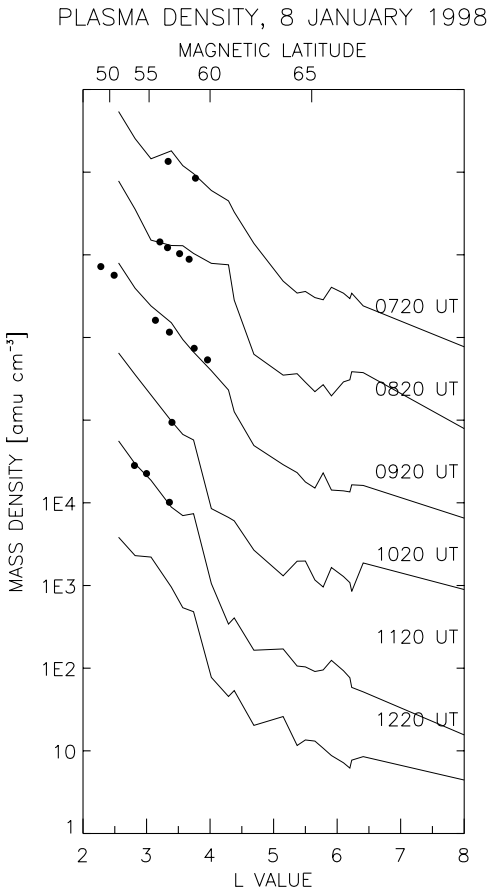

Figure 7b. Plasma mass density profiles for times shown in Figure 7a, separated by one order of magnitude. Circles represent VLF electron density measurements at the same UT.

0900–1000 UT on 11 January 1998 and the model profiles described by *Poulter and Allan* [1986] and *Carpenter and Anderson* [1992]. The plasmapause is represented with a width of 0.2 R_E. Filled circles denote the projection to the equatorial plane of hypothetical ground magnetometer stations separated in geographic latitude by about 110 km. Observationally we find that this is about the optimum station separation at which resonance signatures are most reliably detected. More closely spaced stations may view overlapping flux tubes while larger station separations diminish the spatial resolution. The dashed lines in Figure 9 represent a model density trough of the form described by *Carpenter et al.* [2000].

4.1.1. Cross-Phase Signature of the Plasmapause

[67] The variation in ULF wave phase and amplitude across locally resonant field lines in the plasmatrough, plasmapause and plasmasphere was described by *Orr and Hanson* [1981]. However, the cross-phase, power difference and power ratio spectra measured between two magnetometers at slightly different L values depend on how the Alfvén velocity varies between the field line apexes. A nonlinear variation in Alfvén velocity on this scale distorts the phase and amplitude variations, and two field lines mapping to the same eigenfrequency straddling the plasmapause will show near-zero cross-phase.

[68] The dotted horizontal lines in the bottom panel of Figure 9 illustrate how this may occur across the equatorward or poleward boundary of the plasmapause. Such phase "drop-outs" provide a means of identifying the plasmapause position [*Milling et al.*, 2001]. Cross-phase 'drop-outs' are represented in Figures 5a, 5b, and 7a by data points plotted on the abscissa. Similarly, the cross-phase is reduced when ground stations map to nearly (but not quite) the same eigenfrequency across a plasmapause boundary. This also increases the measurement uncertainty near the plasmapause, as seen in the same figures.

4.1.2. Spatial Resolution

[69] When using two-station cross-phase and power comparison techniques the spatial resolution is determined by the resonance width and the separation in latitude between the ground magnetometers. The characteristic width of a FLR at middle latitudes is of order 100 km at the ionosphere [*Menk et al.*, 1999, and references therein]. This relates to flux tubes with radial extent in the equatorial plane of about 0.15 R_E (1.0×10^3 km) at $L = 3$ and $\sim$0.4 R_E (2.6×10^3 km) at $L = 5.5$. It will not be possible to resolve structures smaller than this using FLR measurements.

[70] Figure 9 clearly shows that an array of closely spaced ground magnetometers can detect a plasmaspheric density trough of the form represented by the dashed lines, whereas similar features in the plasmatrough, and the width of the plasmapause itself, cannot be resolved in this case. For comparison, the swept frequency receiver on ISEE 1 sampled the plasma density along its orbit every 32 s, resulting in a spatial resolution of order 150 km [*Carpenter and Anderson*, 1992].

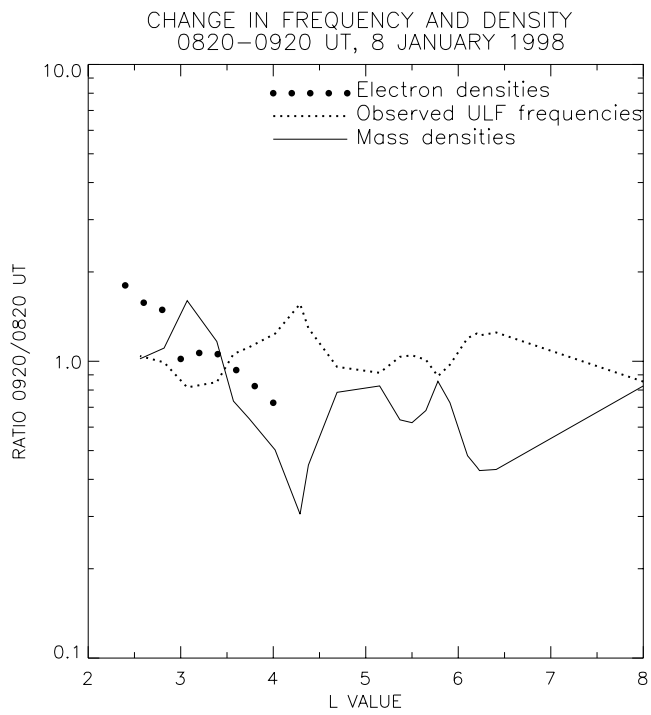

Figure 7c. Change in VLF-derived electron density (filled circles), ULF resonant frequency (dotted line) and ULF-derived mass density (solid line) between 0820 and 0920 UT on 8 January 1998.

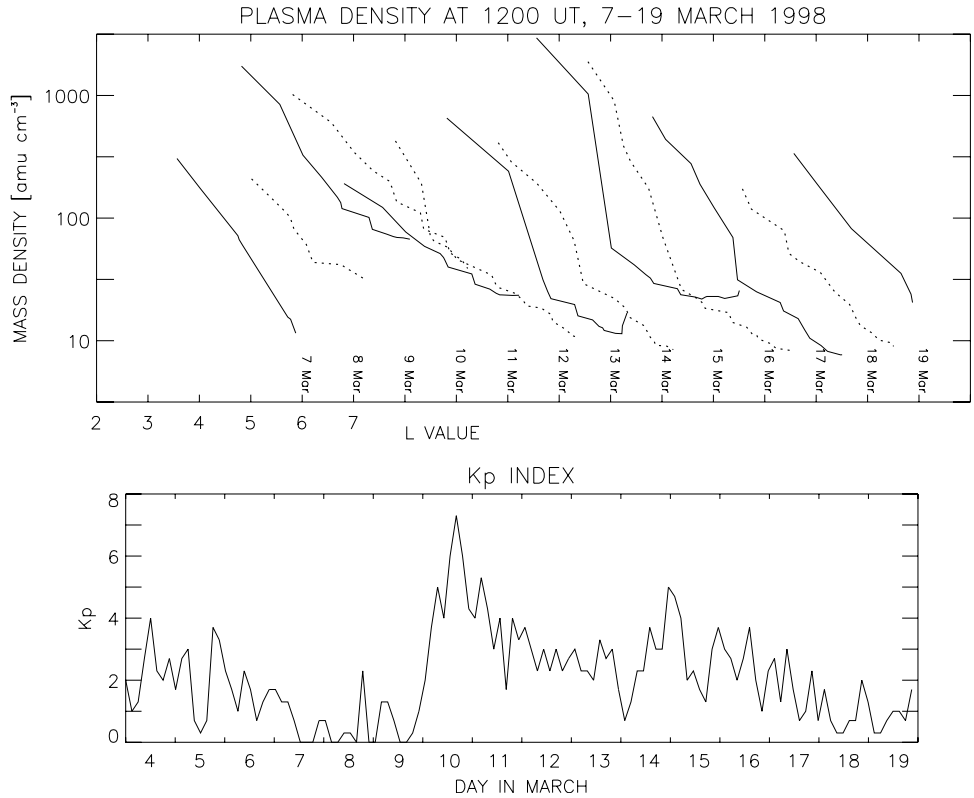

Figure 8. Plasma mass density profiles (top panel) and *Kp* index (bottom) over 7–19 March 1998. Mass densities are for 1200 UT on each day, where each date label in the top panel is at $L = 6.0$ and x-axis tick marks denote steps of 1.0 L.

[71] The spatial resolution when using single station H/D measurements is determined by spatial integration effects [e.g., *Hughes*, 1974; *Poulter and Allan*, 1985]. Consider a downgoing ULF wave that generates Hall currents with horizontal scale size L_i in the ionospheric E-region. The ground magnetic field perturbation can be calculated from the Biot-Savart law and has a larger scale size, $L_g \approx 2H + L_i$, due to the field from the integrated ionospheric current as seen on the ground. The spatial resolution at the ground is therefore about 200 km, no better and possibly worse than that achieved using cross-phase and amplitude subtraction techniques that compare the difference between two stations.

[72] There is a further complication. *Poulter and Allan* [1986] examined the response in the ionosphere and on the ground to transient ULF waves arriving at the plasmapause. They found that the sharp variation in period with latitude in the ionospheric Hall currents is smeared out on the ground as the currents become spatially incoherent. The frequency variation across the plasmapause detected by ground magnetometers is thus smoothed compared to the actual variation, by a factor that depends on the density gradient in the equatorial plane.

[73] In *Poulter and Allan*'s model the resonant frequency measured at the ground increased by ~15% at the equatorward edge of the plasmapause, remained enhanced by ~10% up to 4° further equatorward, and decreased by ~25% at the poleward edge. This smoothing of the plasmapause profile causes underestimation of the density at the equatorward side and overestimation at the poleward edge. Furthermore, *Poulter and Allan* [1986] used a relatively broad (ΔL = 1.0) plasmapause profile, so the smoothing effect will be more pronounced for steeper profiles. Such smoothing appears to be present in the measured profiles shown in Figure 5b.

4.1.3. Cross-Phase Reversal at the Plasmapause

[74] The cross-phase between two ground stations is inverted when these stations map to the portion of the Alfvén velocity profile at the plasmapause where the slope is reversed [*Menk et al.*, 1999]. In Figure 9 this corresponds to the region between $L = 4.5$ and $L = 4.7$. The cross-phase reversal in this region may be used, in principle, to monitor the exact plasmapause location [*Waters*, 2000]. In reality this may be difficult to achieve, because (i) it requires a suitably wide, linear plasmapause to fortuitously straddle the measuring stations; (ii) due to spatial resolution issues discussed above ground magnetometers located precisely at the Alfvén velocity turning points will also map a considerable distance either side of the plasmapause; and (iii) the median dayside plasmapause width of ~0.2 R_E [*Carpenter and Anderson*, 1992] is smaller than the typical spatial resolution of FLR measurements. This is illustrated in Figure 9, where only one measurement station lies on the plasmapause.

4.1.4. Width of the Plasmapause

[75] A survey by *Laakso and Jarva* [2001] of over 6000 Polar spacecraft crossings of the plasmapause found that while the density variation at the nightside plasmapause is usually very sharp, for the dayside plasmapause this is often quite gradual, so that the plasmapause location cannot be

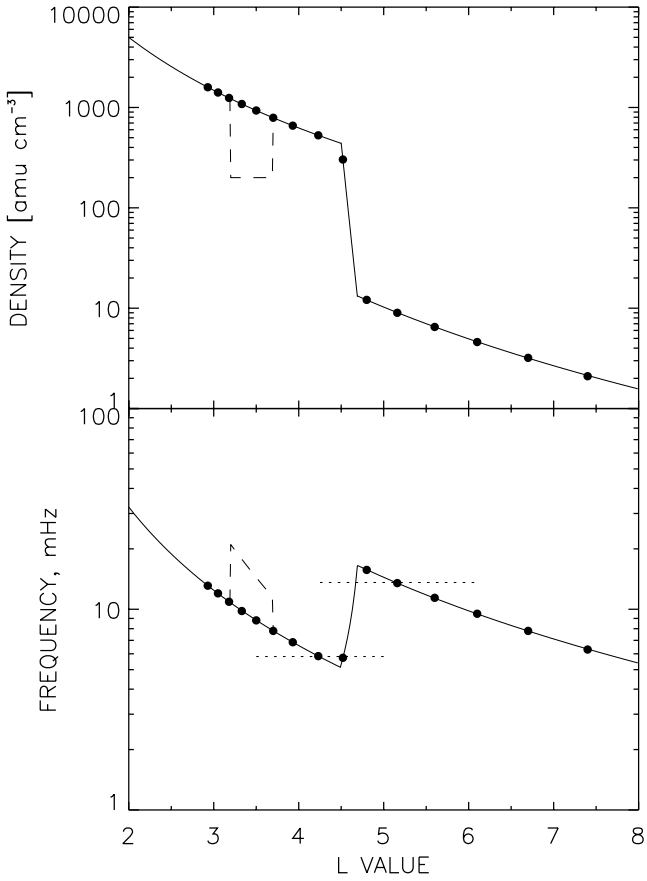

Figure 9. Model profiles of plasma density (top panel) and resonant frequency (bottom) for conditions similar to 0900 UT on 11 January 1998. Filled circles denote L values of (hypothetical) ground stations each separated by 110 km. Dashed line segments illustrate a plasmaspheric density trough. Horizontal dotted lines in bottom panel represent resonances at the same frequency either side of the plasmapause.

defined accurately. Under such circumstances FLR measurements may be able to provide important information on the mass density and its distribution near the plasmapause. Specifically, *Carpenter and Anderson*'s [1992] Figure 7a shows that 5 of 24 'smooth' plasmapause widths between 06–18 MLT exceeded 1500 km. FLR observations with ground magnetometers 100 km apart may therefore resolve a 'smooth' plasmapause in about 20% of cases. At other times FLR measurements will only provide an upper limit on the plasmapause width.

[76] In practice we find that under average and disturbed geomagnetic conditions resonance signatures are readily obtained either side of the plasmapause but only occasionally across it. For comparison, VLF whistler ducts are typically 300–400 km wide in the equatorial plane and are also unlikely to straddle the plasmapause [*Smith*, 2001]. One advantage of the ULF resonance observations, however, is that they relate to the dayside where the plasmapause is less accessible to whistler measurements.

4.1.5. Local Time Distribution

[77] We find that resonances are observable on most days, even at magnetically quiet times such as 1 January 1998, when power levels are low. Resonant structure is usually evident between about 03 and 16 MLT, but can occasionally extend over virtually the entire 24-hour day, particularly at higher latitudes where power levels are higher. Resonant structure is also apparent for Pi2 pulsations at substorm onset, and could in principle be used to estimate mass densities in the bulge region.

4.1.6. Amplitude Variation Across the Plasmapause

[78] The density variation at the plasmapause can reflect a substantial fraction of incoming wave energy. The reflection condition is given by *Allan and Knox* [1979]:

$$R \approx \left[\frac{A_1 - A_2}{A_1 + A_2}\right]^2 \tag{1}$$

where A_1 and A_2 are the Alfvén speeds just inside and just outside the plasmapause respectively. For instance, on 11 January mass density drops across the plasmapause by a factor of about 40, so $R \approx 0.52$. Accordingly, the power difference or ratio between two stations spanning the plasmapause shows an offset that may also be used to detect the plasmapause position. Furthermore, the plasmapause may affect the FLR decay or damping rate in a characteristic manner [*Poulter and Allan*, 1986].

4.2. Effect of Heavy Ions

[79] The shape and dynamic behavior of the plasmapause may be significantly different for ions compared to electrons. For example, Figure 1a of *Singh and Horwitz* [1992] shows in situ observations where the O^+ density near the plasmapause varies markedly following a geomagnetic storm.

[80] Field line resonance observations can be used to estimate the proportion of heavy ions in two ways. The first simply involves comparison of ULF-derived mass densities with VLF electron densities [*Menk et al.*, 1999], with suitable corrections for local time or longitudinal effects. We consider two examples.

[81] Figure 3 shows that on 1 January the Halley electron densities at $L \sim 4$ at 0700 LT were almost double the corresponding mass densities ~0920 LT. Figure 4 demonstrates that the mass density profiles do not change significantly between these times. In early January the Halley ionosphere is continuously sunlit and photoelectron production is enhanced. Because Halley is at relatively low geographic latitude, horizontal ionospheric winds can drive the extra electrons up field lines, increasing the equatorial electron density by a factor of ~2.3 at $L = 2.5$ at that longitude [*Clilverd et al.*, 1991]. The electron and mass densities seen in Figure 3 therefore seem reasonable for a predominantly electron-proton plasma. On 8 January, following a short magnetic storm, the whistler electron densities are similar to the mass densities at the same UT (e.g., Figure 7b). If we ignore the LT separation between the whistler and ULF observatories these measurements could be accounted for by a plasma comprising, for example, 75% H^+, 20% He^+ and 5% O^+ by number at $L = 2.5$.

[82] The second method for estimating the plasma composition involves comparing the frequency of resonance harmonics. The presence of heavy ions results in irregular spacing of harmonics [*Troitskaya and Gul'yel'mi*, 1970; *Poulter et al.*, 1988]. *Price et al.* [1999] showed how the

harmonic spacing may be used to obtain the plasma density at several points along a low latitude field line, while *Menk et al.* [1999] estimated the plasma density power law index from the harmonic spacing of mid-latitude FLRs.

[83] Using 48 months of ion composition data from GEOS 1 and 2, *Young et al.* [1982] statistically described the variation in ion density near geostationary orbit with geomagnetic and solar activity. They considered the energy-per-charge range 0.9–15.9 keV/e. From their results, we may expect the O^+/H^+ ratio in ion mass density to be as high as 0.75 for $Kp = 6.3$ on 7 January, reducing to 0.21 when $Kp = 1$ on 8 January. In contrast, *Young et al.* [1982] found no significant dependence on magnetic activity for He^+ density. It therefore seems likely that the higher mass densities observed on 8 January can be attributed to enhanced O^+ densities on that day.

[84] The mass density profiles presented in Figure 8 show the steepest plasmapause on 15 March, some days after *Kp* reached 7+ and following moderate magnetic activity. Clearly the plasmapause shape varies in a complex manner and will be strongly influenced by changes in the heavy ion concentration associated with loss and refilling processes. FLR measurements allow plots of this type to produced for essentially all local day times. When combined with ground-based or in situ electron density data, it would be possible to systematically examine the variation in heavy ion mass loading during a storm cycle.

4.3. Quiet-Time Plasmapause

[85] Plasma mass density measurements were presented for a typical quiet day in section 3.1. Figure 3 shows that the latitude of the vestigial plasmapause determined with ULF resonances generally agrees with the *Orr and Webb* [1975] empirical prediction. The ULF-derived mass densities generally have uncertainty <20% and agree well with electron density profiles for similar geomagnetic conditions [*Carpenter and Anderson*, 1992]. There is also evidence in Figure 4 of density perturbations evolving in the outer plasmasphere, around $L = 4$. It is clear that under quiet conditions FLR measurements are able to provide useful mass density information throughout the magnetosphere, including in the vicinity of the plasmapause.

4.4. Source of the Pulsation Signals

[86] Ground-based monitoring of the magnetospheric plasma using FLRs requires a broadband source of wave energy. We find that it is possible to determine the radial density profile using FLRs on most days. The resonant frequency at the plasmapause typically extends up to 20 mHz, as modeled by *Poulter and Allan* [1986], but not generally up to 40 mHz as suggested by *Orr and Hanson* [1981]. However, signals above the resonant frequency are often present near the plasmapause.

[87] Spacecraft measurements [e.g., *Takahashi and McPherron*, 1982] show that a continuum of resonances is present throughout the magnetosphere at least some of the time. Our observations and previous cross-phase studies [*Waters et al.*, 1991; *Menk et al.*, 1999] demonstrate that FLRs can be detected even when there is little power at those frequencies. Broadband waves may be produced by impulsive sources, but it is not apparent whether this can explain FLRs observed at quiet times. Other possible source mechanisms include the Kelvin-Helmholtz instability, magnetospheric cavity and waveguide modes [*Mann et al.*, 1999], and penetration into the magnetosphere of compressional mode waves generated by the ion-cyclotron mechanism in the upstream solar wind [e.g., *Howard and Menk*, 2001]. Cavity and waveguide modes may produce a comb of discrete frequencies in the magnetosphere, while the frequency of upstream waves is determined by the IMF magnitude and cone angle. We find that pulsation power in the magnetosphere is strongly dependent on IMF cone angle, but resonances can be reliably detected across a range of frequencies (i.e., latitudes) under a variety of cone angle conditions.

4.5. Detection of Density Irregularities and Temporal Variations

[88] As illustrated in Figure 9, plasmaspheric density depletions of the form described by *Carpenter et al.* [2000] can be readily detected with FLR measurements. A depletion in mass density by a factor of 2–2.5 near $L = 3.6$ is seen in the 0900 and 1200 UT profiles on 11 January (Figure 5b). The radial extent of the depletion is 0.2–0.35 R_E. By 1500 UT the depletion can no longer be resolved, meaning that its radial extent then is <0.2 R_E. We have no information on the longitudinal extent of this depletion, and it may be co-rotating. Although this feature is somewhat smaller than the electron density depletions reported by *Carpenter et al.* [2000], it is clear that FLR measurements can provide new information on plasmaspheric density structures.

[89] For a given station pair, resonance signatures are most clearly identified under quiet magnetic conditions. With increasing activity the cross-phase and power comparison spectra become less ordered and the uncertainty in estimating the resonant frequency increases. This is probably due to the formation of plasma density irregularities with scale sizes and on time scales less than the spatial and temporal resolution.

[90] The temporal resolution of ULF-based density measurements depends on the FFT window length used to produce each cross-phase and power comparison spectrum. We adjusted the window start and end time times in accord with pulsation activity, using shorter windows when magnetic activity increases, and longer windows as pulsation frequency decreases. Temporal resolution is generally between 20 and 60 min. Under magnetically disturbed conditions the plasma distribution in the sampled region may change significantly during this time, resulting in extra features and distortions in the cross-phase and power comparison spectra. This is depicted in Figures 5 and 7 by measurements with particularly large error bars, or error bars where no measured value is shown.

[91] Occasionally more than one distinct resonance signature can be simultaneously identified in the cross-phase and power difference spectra. These 'secondary resonance' features are not harmonically related to the primary FLR and typically have lower power. They may appear or disappear from one spectrum to the next, or may be present for a few hours. Considering the spatial and temporal resolution of the spectra, such secondary features may either be due to a localized density perturbation (scale size <field of view) or a perturbation evolving or moving through the

field of view during the analysis period. Thus, although FLR techniques cannot resolve such structures, they can at least suggest their presence.

4.6. Effects of Solar Wind Variations

[92] Here we consider possible causes of the sudden reductions in ULF-derived mass density observed in connection with solar wind pressure enhancements on 8 and 31 January.

[93] The pressure balance along a flux tube governs the ionosphere-magnetosphere flux interchange. Although this is controlled by many factors [e.g., *Hanson and Ortenburger*, 1961; *Poulter et al.*, 1988], ionization flow from the magnetosphere to the ionosphere enhances the F-region critical frequency, foF2, within 20 min of a substorm onset [*Park*, 1973]. After about one hour inward $\mathbf{E} \times \mathbf{B}$ motion of plasma causes a reduction in the height of F2 layer peak. We examined ionospheric data obtained from the World Data Centre for Solar-Terrestrial Science (Sydney; http://www.ips.gov.au/wdc-sts/) for various observatories near the IMAGE meridian, including Juliusruh/Rugen (L = 2.7), Uppsala (L = 3.3), Lerwick (L = 3.6), Lycksele (L = 4.5) and Kiruna (L = 5.5) for the times of interest on 8 January. It was not possible to discern any variations in foF2 or hmF2 that could be clearly related to the magnetospheric mass density decreases or the solar wind pressure enhancements on that day. Therefore the observed changes in the density profiles are unlikely to be due to magnetosphere-ionosphere coupling effects.

[94] Mass densities derived from FLR measurements are affected by motion of magnetic field lines in response to magnetospheric distortion by solar wind pressure variations. Considering the time of flight approximation [e.g., *Orr and Matthew*, 1971], the resonant frequency ω_r depends on density ρ according to

$$\omega_r \propto \int \frac{\mathbf{B}}{\sqrt{\rho}} \cdot \frac{1}{ds}. \tag{2}$$

A change in resonant frequency may therefore be caused by changes in **B** and field line length as well as changes in density. A second mechanism is also important. By Faraday's law, variations in **B**, $d\mathbf{B}/dt$, for a given field line induce changes in **E** that can also drive cross-L plasma motion.

[95] The sudden solar wind pressure enhancement at 0831 UT on 8 January resulted in magnetospheric compression and global *DP* 2-like impulses in ground magnetometer records (not shown). It is clear from Figure 7c that the solar wind pressure enhancement caused a redistribution of plasma on a time scale of less than one hour. The difference between the observed variation in mass density and electron density may be related the presence of heavy ions or longitudinal differences in the magnetospheric electric fields and convective drifts between the flux tubes sampled by the IMAGE magnetometers and the Halley VLF receiver.

[96] It is likely that undershielding effects (see section 1) dominate plasma motion beyond L = 3.3 on 8 January between 0820 and 0920 UT. The sudden solar wind pressure enhancement at 0831 UT was accompanied by a strong decrease in B_z (Figure 6). We therefore anticipate that convection electric fields penetrating to the inner magnetosphere would drive sunward cross-L $\mathbf{E} \times \mathbf{B}$ drift of flux tubes, resulting in a decrease in mass and electron density between L = 3.3 and the plasmapause ($L \sim 4.3$). A different effect is required to explain the pronounced increase in electron density for $L < 3.0$.

[97] The sudden formation of *DP* 2 currents should also generate polar electrojets that can be detected with high latitude magnetometers and are characterized by the AE index. Information on electrojet locations is available from the IMAGE magnetometer array web site. In averaged data for 1998 no electrojet is present at 0830 UT, and the eastward electrojet usually appears around 1100 UT between $\sim$70–74° latitude. On 8 January eastward electrojet flows appeared briefly at 0830 UT, with the poleward boundary at 76° and the equatorward boundary moving from 72–74° geomagnetic latitude. The electrojet flows became sustained after 1030 UT, when the poleward boundary was around 76° and the equatorward boundary oscillated between 71–73° latitude. The local AU and AE indices show brief but significant increases in connection with the first and second solar wind enhancements.

[98] In summary, the sudden increase in solar wind pressure and southward turning in the IMF B_Z on 8 January 1998 resulted in magnetospheric compression and enhanced magnetospheric convection electric fields. The former were identified by impulses on ground magnetometers. However, the main effect on the magnetospheric plasma seems due to the penetration electric field that likely caused cross-L drifts and observed decreases in plasma density. The magnitude of these changes is significantly larger for ions than for electrons, probably due to enhanced O^+ concentrations, and is maximum at the plasmapause.

5. Conclusions

[99] This study has explored the use of ground magnetometer data to obtain field line eigenfrequencies and hence mass densities throughout the magnetosphere, in particular around dayside plasmapause. We examined data from January and March 1998 from the combined IMAGE and SAMNET arrays with cross-phase and power comparison techniques, presenting case studies of three selected days.

[100] Under geomagnetically quiet conditions FLR-derived plasma density profiles often do not show a sharp plasmapause and closely resemble electron density profiles obtained under similar conditions, suggesting a primarily electron-proton plasma. The resonances are not apparent in power spectra but are clearly evident in cross-phase spectra. Sufficient ULF energy exists in the magnetosphere to excite the resonance continuum over a broad range of frequencies even at quiet times. The measured latitudes of the plasmapause and the magnetopause agree well with empirical estimates. The calculated mass densities are significantly lower than simultaneous whistler-derived electron densities from a longitude sector in the southern hemisphere that is continuously sunlit. Uncertainty in the mass densities is typically <20%.

[101] During storm recovery phase a distinct plasmapause is present in the FLR mass density profiles. It is possible to resolve the dayside plasmapause itself in about 20% of cases, and most often the resonance measurements only provide an upper limit to the plasmapause width. Further-

more, the calculated densities are smoothed near the plasmapause edges due to spatial integration effects. Comparison of the mass and electron densities allows the heavy ion mass loading to be estimated. Observed variations in the shape and position of the dayside plasmapause are not predicted by empirical models. Plasmaspheric density depletions with radial width $\geq 0.15\ R_E$ at $L = 3$ and $\geq 0.4\ R_E$ at $L = 5.5$ can be resolved. The presence of complex plasma features that cannot be resolved can frequently be inferred. These are likely due to density perturbations with relatively small scale sizes, and features that undergo significant change on a time scale of $\sim$30–60 min.

[102] On disturbed days sudden changes in mass density may be observed across widely spaced L-values within $\sim$20 min of solar wind pressure variations. Whistler-derived electron densities also show variation but do not track the changes in mass density in the case examined. The solar wind-related density variations probably arise from a combination of cross-L drifts driven by enhanced magnetospheric convection fields, the effect of field line distortion due to magnetospheric compression, and longitudinal variations in plasma dynamics between the ULF and VLF recording stations.

[103] Field line resonances occur daily. The analysis of FLR data from existing magnetometer arrays permits investigation of aspects of the dayside plasmasphere that are still poorly understood. Issues for future work include detailed investigation of density depletions and other perturbations in the plasmasphere; monitoring the evolution of the storm-time plasmapause, and hence the role of heavy ion loss and refilling processes; and examining in detail the response of plasma in the dayside magnetosphere to solar wind variations. Furthermore, the extensive existing suites of magnetometer data permit retrospective studies of focus intervals.

[104] **Acknowledgments.** The IMAGE magnetometer data are collected as a Finnish-German-Norwegian-Polish-Russian-Swedish project and we thank those institutes who maintain the array. IMAGE data were kindly provided by the Finnish Meteorological Institute. SAMNET is a PPARC (U.K.) National Facility now operated by the University of Lancaster. The 210MM array is operated by K. Yumoto (Kyushu University), and data were kindly supplied by K. Shiokawa (STELab, Nagoya University). Aspects of this work were supported by the Australian Research Council, the University of Newcastle, and the Cooperative Research Centre for Satellite Systems through the Commonwealth of Australia CRC Program. FWM acknowledges the hospitality of the University of York, U.K., during much of this study.

[105] Lou-Chuang Lee thanks Jeffrey Hughes and Kazue Takahashi for their assistance in evaluating this paper.

References

Allan, W., and F. B. Knox (1979), A dipole model for axisymmetric Alfvén waves with finite ionosphere conductivities, *Planet. Space Sci.*, *27*, 79–85.

Anderson, B. J., M. J. Engebretson, and L. J. Zanetti (1989), Distortion effects in spacecraft observations of MHD toroidal standing waves: Theory and observations, *J. Geophys. Res.*, *94*, 13,425–13,445.

Angerami, J. J. (1970), Whistler duct properties deduced from VLF observations made with the OGO 3 satellite near the magnetic equator, *J. Geophys. Res.*, *75*, 6115–6135.

Balmforth, H. F., R. J. Moffett, A. J. Smith, and G. J. Bailey (1994), The effect of disturbed-time electric fields on the inner plasmasphere, *Ann. Geophys.*, *12*, 296–303.

Bezrukikh, V. V., M. I. Verigin, G. A. Kotova, L. A. Lezhen, Y. I. Venediktov, and J. Lemaire (2001), Dynamics of the plasmasphere and plasmapause under the action of geomagnetic storms, *J. Atmos. Sol. Terr. Phys.*, *63*, 1179–1184.

Carpenter, D. L. (1970), Whistler evidence of the dynamic behavior of the duskside bulge in the plasmasphere, *J. Geophys. Res.*, *75*, 3837–3847.

Carpenter, D. L., and R. R. Anderson (1992), An ISEE/whistler model of equatorial electron density in the magnetosphere, *J. Geophys. Res.*, *97*, 1097–1108.

Carpenter, D. L., and J. Lemaire (1997), Erosion and recovery of the plasmasphere in the plasmapause region, *Space Sci. Rev.*, *80*, 153–179.

Carpenter, D. L., and C. G. Park (1973), On what ionospheric workers should know about the plasmapause-plasmasphere, *Rev. Geophys.*, *11*, 133–154.

Carpenter, D. L., R. R. Anderson, W. Calvert, and M. B. Moldwin (2000), CRRES observations of density cavities inside the plasmasphere, *J. Geophys. Res.*, *105*, 23,323–23,338.

Chappell, C. R. (1974), Detached plasma regions in the magnetosphere, *J. Geophys. Res.*, *79*, 1861–1870.

Chappell, C. R., K. K. Harris, and G. W. Sharp (1971), The dayside of the plasmasphere, *J. Geophys. Res.*, *76*, 7632–7647.

Chi, P. J., C. T. Russell, S. Musman, W. K. Peterson, G. Le, V. Angelopoulos, G. D. Reeves, M. B. Moldwin, and F. K. Chun (2000), Plasmaspheric depletion and refilling associated with the September 25, 1998 magnetic storm observed by ground magnetometers at $L = 2$, *Geophys. Res. Lett.*, *27*, 633–636.

Clilverd, M. A., A. J. Smith, and N. R. Thomson (1991), The annual variation in quiet time plasmaspheric electron density determined from whistler mode group delays, *Planet. Space Sci.*, *39*, 1059–1067.

Clilverd, M. A., B. Jenkins, and N. R. Thomson (2000), Plasmaspheric storm time erosion, *J. Geophys. Res.*, *105*, 12,997–13,008.

Clilverd, M. A., et al. (2003), In situ and ground-based intercalibration measurements of plasma density at $L = 2.5$, *J. Geophys. Res.*, *108*(A10), 1365, doi:10.1029/2003JA009866.

Décréau, P. M. E., J. Lemaire, C. R. Chappell, and J. H. Waite Jr. (1986), Nightside plasmapause positions observed by DE-1 as a function of geomagnetic indices: Comparison with whistler observations and model calculations, *Adv. Space Res.*, *6*, 209–214.

Denton, R. E., and D. L. Gallagher (2000), Determining the mass density along magnetic field lines from toroidal eigenfrequencies, *J. Geophys. Res.*, *105*, 27,717–27,725.

Farrugia, C. J., M. P. Freeman, S. W. H. Cowley, D. J. Southwood, M. Lockwood, and A. Etemadi (1989), Pressure-driven magnetopause motions and attendant response on the ground, *Planet. Space Sci.*, *37*, 589–607.

Gallagher, D. L., P. D. Craven, and R. H. Comfort (2000), Global core plasma model, *J. Geophys. Res.*, *105*, 18,819–18,833.

Goldstein, J., R. E. Denton, M. K. Hudson, E. G. Miftakhova, S. L. Young, J. D. Menietti, and D. L. Gallagher (2001), Latitudinal density dependence of magnetic field lines inferred from Polar plasma wave data, *J. Geophys. Res.*, *106*, 6195–6201.

Goldstein, J., R. W. Spiro, P. H. Reiff, R. A. Wolf, B. R. Sandel, J. W. Freeman, and R. L. Lambour (2002), IMF-driven overshielding electric field and the origin of the plasmaspheric shoulder of May 24, 2000, *Geophys. Res. Lett.*, *29*(16), 1819, doi:10.1029/2001GL014534.

Gul'yel'mi, A. V. (1966), Plasma concentration at great heights according to data on toroidal fluctuations of the magnetosphere, *Geomagn. Aeron.*, *6*, 98–101.

Gurnett, D. A., R. R. Anderson, F. L. Scarf, R. W. Fredricks, and E. J. Smith (1979), Initial results from the ISEE-1 and -2 plasma wave investigation, *Space Sci. Rev.*, *23*, 103–122.

Hanson, W. B., and I. B. Ortenburger (1961), The coupling between the protonosphere and the normal F region, *J. Geophys. Res.*, *86*, 1425–1435.

Ho, D., and L. C. Bernard (1973), A fast method to determine the nose frequency and minimum group delay of a whistler when the causative spheric is unknown, *J. Atmos. Terr. Phys.*, *35*, 881–887.

Horwitz, J. L., R. H. Comfort, and C. R. Chappell (1984), Thermal ion composition measurements of the formation of the new outer plasmasphere and double plasmapause during storm recovery phase, *Geophys. Res. Lett.*, *11*, 701–704.

Horwitz, J. L., R. H. Comfort, and C. R. Chappell (1990), A statistical characterization of plasmasphere density structure and boundary locations, *J. Geophys. Res.*, *95*, 7937–7947.

Howard, T. A., and F. W. Menk (2001), Propagation of 10–50 mHz ULF waves at high latitudes, *Geophys. Res. Lett.*, *28*, 231–234.

Hughes, W. J. (1974), The effect of the atmosphere and ionosphere on long period magnetospheric micropulsations, *Planet. Space Sci.*, *22*, 1157–1172.

Laakso, H., and M. Jarva (2001), Evolution of the plasmapause position, *J. Atmos. Sol. Terr. Phys.*, *63*, 1171–1178.

Lühr, H., A. Aylward, S. C. Buchert, A. Pajunpää, K. Pajunpää, T. Holmboe, and S. M. Zalewski (1998), Westward moving dynamic substorm features observed with the IMAGE magnetometer network and other ground-based instruments, *Ann. Geophys.*, *16*, 425–440.

Mann, I. R., A. N. Wright, K. Mills, and V. M. Nakariakov (1999), Excitation of magnetospheric waveguide modes by magnetosheath flows, *J. Geophys. Res.*, *104*, 333–353.

Mathie, R., F. W. Menk, I. R. Mann, and D. Orr (1999), Discrete field line resonances and the Alfvén continuum in the outer magnetosphere, *Geophys. Res. Lett.*, *26*, 659–662.

Maynard, N. C., and A. J. Chen (1971), Isolated cold plasma regions: Observations and their relation to possible production mechanisms, *J. Geophys. Res.*, *80*, 1009–1013.

Menk, F. W., D. Orr, M. A. Clilverd, A. J. Smith, C. L. Waters, and B. J. Fraser (1999), Monitoring spatial and temporal variations in the dayside plasmasphere using geomagnetic field line resonances, *J. Geophys. Res.*, *104*, 19,955–19,970.

Menk, F. W., C. L. Waters, and B. J. Fraser (2000), Field line resonances and waveguide modes at low latitudes: 1. Observations, *J. Geophys. Res.*, *105*, 7747–7761.

Milling, D. K., I. R. Mann, and F. W. Menk (2001), Diagnosing the plasmapause with a network of closely spaced ground-based magnetometers, *Geophys. Res. Lett.*, *28*, 115–118.

Moldwin, M. B., M. T. Thomsen, S. J. Bame, D. J. McComas, and K. R. Moore (1994), An examination of the structure and dynamics of the outer plasmasphere using multiple geosynchronous satellites, *J. Geophys. Res.*, *99*, 11,475–11,481.

Moldwin, M. B., M. T. Thomsen, S. J. Bame, D. McComas, and G. D. Reeves (1995), The fine-scale structure of the outer plasmasphere, *J. Geophys. Res.*, *100*, 8021–8029.

Mosier, S. R., M. L. Kaiser, and L. W. Brown (1973), Observations of noise bands associated with the upper hybrid resonance by the Imp 6 radio astronomy experiment, *J. Geophys. Res.*, *78*, 1673–1679.

Olsen, R. C. (1982), The hidden ion population of the magnetosphere, *J. Geophys. Res.*, *87*, 3481–3488.

Orr, D., and H. W. Hanson (1981), Geomagnetic pulsation phase patterns over an extended latitudinal array, *J. Atmos. Terr. Phys.*, *43*, 899–910.

Orr, D., and J. A. D. Matthew (1971), The variation of geomagnetic micropulsation periods with latitude and the plasmapause, *Planet. Space Sci.*, *19*, 897–904.

Orr, D., and D. C. Webb (1975), Statistical studies of geomagnetic pulsations with periods between 10 and 70 sec and their relationship to the plasmapause region, *Planet. Space Sci.*, *23*, 1169–1178.

Park, C. G. (1973), Whistler observations of the depletion of the plasmasphere during a magnetospheric substorm, *J. Geophys. Res.*, *78*, 672–683.

Park, C. G., D. L. Carpenter, and D. B. Wiggin (1978), Electron density in the plasmasphere: Whistler data on solar cycle, annual, and diurnal variations, *J. Geophys. Res.*, *83*, 3137–3144.

Poulter, E. M., and W. Allan (1985), Transient ULF pulsation decay rates observed by ground based magnetometers: The contribution of spatial integration, *Planet. Space Sci.*, *33*, 607–616.

Poulter, E. M., and W. Allan (1986), The ground magnetic fields of transient ULF pulsations at the plasmapause, *Planet. Space Sci.*, *34*, 1073–1079.

Poulter, E. M., M. K. Andrews, G. J. Bailey, and R. J. Moffett (1984), Radial plasma drifts deduced from VLF whistler mode signals: A modelling study, *Planet. Space Sci.*, *32*, 525–533.

Poulter, E. M., W. Allan, and G. J. Bailey (1988), ULF pulsation eigenperiods within the plasmasphere, *Planet. Space Sci.*, *36*, 185–196.

Price, I. A., C. L. Waters, F. W. Menk, G. J. Bailey, and B. J. Fraser (1999), A technique to investigate plasma mass density in the topside ionosphere using ULF waves, *J. Geophys. Res.*, *104*, 12,723–12,735.

Rees, J. M., C. R. Wilford, R. J. Moffett, Z. C. Dent, I. R. Mann, and D. K. Milling (2001), Wavelet analysis of magnetometer data—Preliminary results, in *Sheffield Space Plasma Meeting: Multipoint Measurements Versus Theory*, *Eur. Space Agency Spec. Publ.*, *ESA-SP 492*, 151–156.

Roberts, W. T., Jr., J. L. Horwitz, R. H. Comfort, C. R. Chappell, J. H. Waite Jr., and J. L. Green (1987), Heavy ion density enhancements in the outer plasmasphere, *J. Geophys. Res.*, *92*, 13,499–13,512.

Sandel, B. R., R. A. King, W. T. Forrester, D. L. Gallagher, A. L. Broadfoot, and C. C. Curtis (2001), Initial results from the IMAGE extreme ultraviolet imager, *Geophys. Res. Lett.*, *28*, 1439–1442.

Saxton, J. M., and A. J. Smith (1989), Quiet time plasmaspheric electric fields and plasmasphere-ionosphere coupling fluxes at $L = 2.5$, *Planet. Space Sci.*, *37*, 283–293.

Saxton, J. M., and A. J. Smith (1991), Electric fields at $L = 2.5$ during geomagnetically disturbed conditions, *Planet. Space Sci.*, *39*, 1305–1320.

Scarf, F. L., and C. R. Chappell (1973), An association of magnetospheric whistler dispersion characteristics with changes in local plasma density, *J. Geophys. Res.*, *78*, 1597–1602.

Schulz, M. (1996), Eigenfrequencies of geomagnetic field lines and implications for plasma-density modeling, *J. Geophys. Res.*, *101*, 17,385–17,397.

Senior, C., and M. Blanc (1984), On the control of magnetospheric convection by the spatial distribution of ionospheric conductivities, *J. Geophys. Res.*, *89*, 261–284.

Singer, H. J., D. J. Southwood, R. J. Walker, and M. G. Kivelson (1981), Alfvén wave resonances in a realistic magnetospheric magnetic field geometry, *J. Geophys. Res.*, *86*, 4589–4596.

Singh, N., and J. L. Horwitz (1992), Plasmasphere refilling: Recent observations and modeling, *J. Geophys. Res.*, *97*, 1049–1079.

Smith, A. J. (2001), Whistler observations of the plasmasphere/plasmapause from stations of the British Antarctic Survey, *J. Atmos. Sol. Terr. Phys.*, *63*, 1149–1156.

Southwood, D. J. (1974), Some features of field line resonances in the magnetosphere, *Planet. Space Sci.*, *22*, 482–491.

Takahashi, K., and R. L. McPherron (1982), Harmonic structure of Pc3-4 pulsations, *J. Geophys. Res.*, *87*, 1504–1516.

Taylor, J. P. H., and A. D. M. Walker (1984), Accurate approximate formulae for toroidal standing hydromagnetic oscillations in a dipolar geomagnetic field, *Planet. Space Sci.*, *32*, 1119–1124.

Troitskaya, V. A., and A. V. Gul'yel'mi (1970), Hydromagnetic diagnostics of plasma in the magnetosphere, *Ann. Geophys.*, *26*, 893–902.

Tsyganenko, N. A., and D. P. Stern (1996), Modeling the global magnetic field of the large-scale Birkeland current systems, *J. Geophys. Res.*, *101*, 27,187–27,198.

Vellante, M., U. Villante, R. Core, A. Best, D. Lenners, and V. A. Pilipenko (1993), Simultaneous geomagnetic pulsation observations at two latitudes: Resonant mode characteristics, *Ann. Geophys.*, *11*, 734–741.

Vellante, M., M. De Lauretis, M. Förster, S. Lepidi, B. Zieger, U. Villante, V. A. Pilipenko, and B. Zolesi (2002), Geomagnetic field line resonances at low latitudes: Pulsation event study of 16 August 1993, *J. Geophys. Res.*, *107*(A5), 1060, doi:10.1029/2001JA900123.

Walker, A. D. M. (1978), Formation of whistler ducts, *Planet Space Sci.*, *26*, 375–379.

Walker, A. D. M., J. M. Ruohoniemi, K. B. Baker, R. A. Greenwald, and J. C. Samson (1992), Spatial and temporal behaviour of ULF pulsations observed by the Goose Bay HF radar, *J. Geophys. Res.*, *97*, 12,187–12,202.

Waters, C. L. (2000), ULF resonance structure in the magnetosphere, *Adv. Space Res.*, *25*, 1541–1558.

Waters, C. L., F. W. Menk, and B. J. Fraser (1991), The resonance structure of low latitude Pc3 geomagnetic pulsations, *Geophys. Res. Lett.*, *18*, 2293–2296.

Yeoman, T. K., D. K. Milling, and D. Orr (1990), Pi2 polarization patterns on the U.K. Sub-Auroral Magnetometer Network (SAMNET), *Planet. Space Sci.*, *38*, 589–602.

Young, D. T., H. Balsinger, and J. Geiss (1982), Correlations of magnetospheric ion composition with geomagnetic and solar activity, *J. Geophys. Res.*, *87*, 9077–9096.

Yumoto, K., Y. Tanaka, T. Oguti, K. Shiokawa, Y. Yoshimura, A. Isono, B. J. Fraser, F. W. Menk, K. J. W. Lynn, and M. Seto (1992), Globally coordinated magnetic observations along 210° magnetic meridian during the STEP period: 1. Preliminary results of low-latitude Pc3, *J. Geomagn. Geoelectr.*, *44*, 261–276.

M. A. Clilverd and A. J. Smith, British Antarctic Survey, Madingley Road, Cambridge CB3 0ET, UK. (macl@bas.ac.uk; ajsm@bas.ac.uk)

I. R. Mann and D. K. Milling, Department of Physics, University of Alberta, Edmonton, Alberta, Canada T6G 2J1. (imann@space.ualberta.ca; dmilling@space.ualberta.ca)

F. W. Menk and C. L. Waters, School of Mathematical and Physical Sciences and CRC for Satellite Systems, University of Newcastle, Callaghan, N.S.W. 2308, Australia. (fred.menk@physics.org; physpuls8@cc.newcastle.edu.au)